Article

Cell Reports

Cytosolic Trapping of a Mitochondrial Heat Shock Protein Is an Early Pathological Event in Synucleinopathies

Graphical Abstract

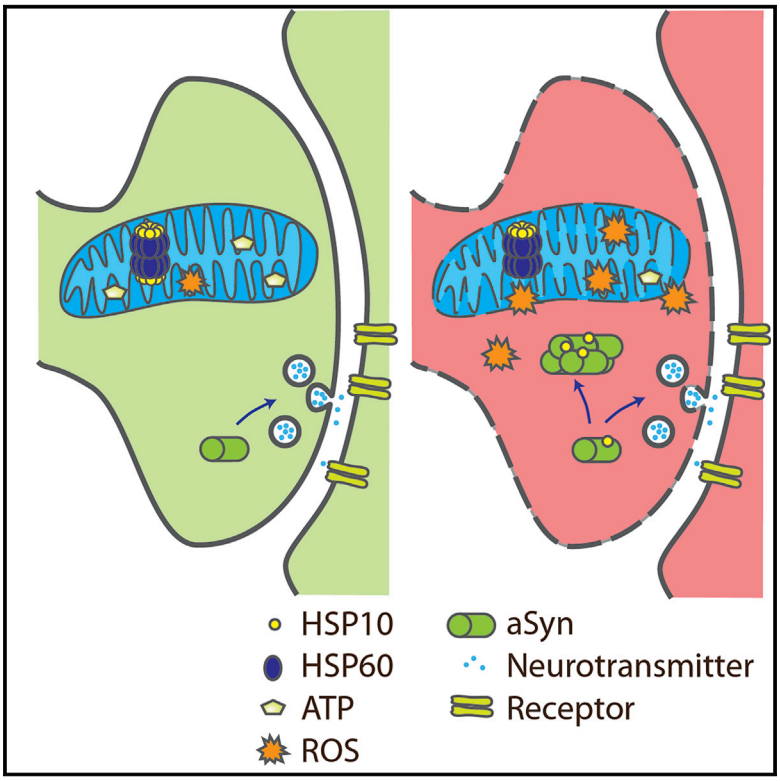

Authors

Éva M. Szegő,
Antonio Dominguez-Meijide,
Ellen Gerhardt, ..., Johannes Attems,
Olaf Jahn, Tiago F. Outeiro

Correspondence

eva.szego@gmail.com (É.M.S.),
touteiro@gwdg.de (T.F.O.)

In Brief

Szegő et al. identify HSP10 as a modulator of alpha-synuclein-induced mitochondrial impairment in striatal synaptosomes. Age-associated increase in the cytosolic and decrease in mitochondrial levels of HSP10 results in a reduction in the levels of SOD2 and of synaptosomal ATP production on demand. HSP10 overexpression delays alpha-synuclein pathology both *in vitro* and *in vivo*.

Highlights

- aSyn sequesters HSP10 in the cytosol and prevents it from acting in the mitochondria
- Overexpression of HSP10 delays aSyn pathology *in vitro* and *in vivo*
- HSP10 modulates aSyn pathology in synaptic terminals

Szegő et al., 2019, Cell Reports *28*, 65–77
July 2, 2019
https://doi.org/10.1016/j.celrep.2019.06.009

CellPress

Cell Reports
Article

Cytosolic Trapping of a Mitochondrial Heat Shock Protein Is an Early Pathological Event in Synucleinopathies

Éva M. Szegő,[1,9,*] Antonio Dominguez-Meijide,[1] Ellen Gerhardt,[1] Annekatrin König,[1] David J. Koss,[2] Wen Li,[7,8] Raquel Pinho,[1] Christiane Fahlbusch,[1] Mary Johnson,[2] Patricia Santos,[1] Anna Villar-Piqué,[1] Tobias Thom,[4] Silvio Rizzoli,[3] Matthias Schmitz,[4] Jiayi Li,[7,8] Inga Zerr,[4] Johannes Attems,[2] Olaf Jahn,[5] and Tiago F. Outeiro[1,2,6,10,*]

[1]Department of Experimental Neurodegeneration, Center for Nanoscale Microscopy and Molecular Physiology of the Brain, University Medical Center, Waldweg 33, Göttingen 37073, Germany
[2]Institute of Neuroscience, Medical School, Newcastle University, Framlington Place, Newcastle upon Tyne NE2 4HH, UK
[3]Department of Neuro- and Sensory Physiology, Center for Nanoscale Microscopy and Molecular Physiology of the Brain, University Medical Center, Humboldtallee 23, Göttingen 37073, Germany
[4]Department of Neurology, University Medical Center and German Center for Neurodegenerative Diseases (DZNE), Robert-Koch Street 40, Göttingen 37075, Germany
[5]Proteomics Group, Max Planck Institute of Experimental Medicine, Center for Nanoscale Microscopy and Molecular Physiology of the Brain, Hermann Rein Street 3, Göttingen 37075, Germany
[6]Max Planck Institute of Experimental Medicine, Hermann Rein Street 3, Göttingen 37075, Germany
[7]Institute of Heath Sciences, China Medical University, 110112 Shenyang, P. R. China
[8]Neural Plasticity and Repair Unit, Wallenberg Neuroscience Center, Department of Experimental Medical Science, BMC A10, 221 84 Lund, Sweden
[9]Present address: Department of Biochemistry, Eötvös Loránd University, Pázmány P. stny 1/c, 1117 Budapest, Hungary
[10]Lead Contact
*Correspondence: eva.szego@gmail.com (É.M.S.), touteiro@gwdg.de (T.F.O.)
https://doi.org/10.1016/j.celrep.2019.06.009

SUMMARY

Alpha-synuclein (aSyn) accumulates in intracellular inclusions in synucleinopathies, but the molecular mechanisms leading to disease are unclear. We identify the 10 kDa heat shock protein (HSP10) as a mediator of aSyn-induced mitochondrial impairments in striatal synaptosomes. We find an age-associated increase in the cytosolic levels of HSP10, and a concomitant decrease in the mitochondrial levels, in aSyn transgenic mice. The levels of superoxide dismutase 2, a client of the HSP10/HSP60 folding complex, and synaptosomal spare respiratory capacity are also reduced. Overexpression of HSP10 ameliorates aSyn-associated mitochondrial dysfunction and delays aSyn pathology *in vitro* and *in vivo*. Altogether, our data indicate that increased levels of aSyn induce mitochondrial deficits, at least partially, by sequestering HSP10 in the cytosol and preventing it from acting in mitochondria. Importantly, these alterations manifest first at presynaptic terminals. Our study not only provides mechanistic insight into synucleinopathies but opens new avenues for targeting underlying cellular pathologies.

INTRODUCTION

A major pathological hallmark of Parkinson's disease (PD) and other synucleinopathies is the presence of intraneuronal inclusions known as Lewy bodies (LBs) and Lewy neurites (LNs). These inclusions are composed mainly of α-synuclein (aSyn) but are known to also contain mitochondrial proteins (Leverenz et al., 2007; Xia et al., 2008). Moreover, mitochondrial dysfunction has been implicated in the pathogenesis of PD: complex I deficiency was detected in the substantia nigra (SN) (Schapira et al., 1989), muscle (Blin et al., 1994), and platelets (Parker et al., 1989) of PD patients, and mutations in several mitochondria-related genes are associated with familial forms of the disease (Corti et al., 2011; Bose and Beal, 2016; Chang et al., 2017).

aSyn is considered primarily a cytoplasmic protein, but recent evidence suggests that it may also accumulate in mitochondria (Hu et al., 2019; Wang et al., 2019) and associate with mitochondria-associated endoplasmic reticulum (ER) (Chinta et al., 2010; Guardia-Laguarta et al., 2014). Whether aSyn plays a physiological role in mitochondria is unclear, but increased aSyn levels inhibit cellular respiration (Chinta et al., 2010; Wang et al., 2019; Zambon et al., 2019), induce mitophagy and mitochondrial fragmentation (Nakamura et al., 2008, 2011), affect mitochondrial Ca^{2+} homeostasis (Calì et al., 2012) and protein import (Di Maio et al., 2016) and turnover (Hu et al., 2019), and reduce mitochondrial membrane potential (Banerjee et al., 2010), suggesting a pathological role that culminates with mitochondrial dysfunction.

Here, we hypothesized that aSyn-dependent mitochondrial dysfunction might initiate in the synapse, because aSyn is likely to start accumulating in the cytoplasm of the presynaptic terminals (Kramer and Schulz-Schaeffer, 2007) and then progress toward the perinuclear region to induce additional cellular pathologies. First, we screened for aSyn-interacting proteins in nerve terminals (striatal synaptosomes) and identified the 10 kDa heat

shock protein (HSP10) as an aSyn interactor and mediator of aSyn-associated mitochondrial dysfunction. Importantly, we obtained detailed insight into the mechanisms through which the accumulation of aSyn, a predominantly cytosolic protein, can induce cellular pathologies by affecting mitochondrial functions. We found that accumulation of aSyn in middle-age transgenic animals sequesters HSP10 in the cytosol, reducing its mitochondrial function in the HSP10/HSP60 complex, which resulted in a reduction in the levels of the client protein superoxide dismutase 2 (SOD2). This led to increased mitochondrial oxidative stress and impaired respiration. Interestingly, improving mitochondrial health by restoring the levels of HSP10 delayed aSyn-induced mitochondrial pathology both *in vitro* and *in vivo*. Our findings provide novel mechanistic information on the molecular underpinnings of PD and might help in designing novel therapeutic strategies for PD and other synucleinopathies.

RESULTS

The HSP10 Chaperonin Interacts with aSyn in Striatal Synaptosomes

aSyn interacts with several synaptic and mitochondrial proteins (Betzer et al., 2015) and affects both synaptic and mitochondrial functions (Guardia-Laguarta et al., 2014; Calo et al., 2016; Di Maio et al., 2016; Faustini et al., 2017; Hu et al., 2019; Wang et al., 2019; Zambon et al., 2019). However, the effects of aSyn in striatal synaptosomal mitochondria have not been addressed in detail. To assess the molecular underpinnings of aSyn-mediated toxicity in striatal mitochondria, we performed a proteomics-based unbiased screen for aSyn-interacting partners in nerve terminals (synaptosomal component). We identified aSyn-interacting proteins in preparations from transgenic overexpressing human aSyn (wild-type aSyn [WTaSyn]) or from control mice. In total, we identified 67 proteins (Table S1). Of those 67 proteins, we selected the HSP10 for further validation, because it forms, together with HSP60, a major folding complex in mitochondria (David et al., 2013). HSP10 is a major hub protein for cellular interactions (Rizzolo et al., 2018) and regulates several mitochondrial functions, including respiration, membrane potential, and reactive oxygen species (ROS) removal. Therefore, even subtle changes in its concentration may affect the functionality of several proteins and cellular functions. The regulation of HSP10 levels in neurological diseases is not well understood (Hickey et al., 2000; Bross et al., 2007; Kim and Lee, 2007; Bie et al., 2016; Bross and Fernandez-Guerra, 2016; Fan et al., 2017), and to our knowledge, this has not been investigated in the context of synucleinopathies. To assess whether the level of HSP10 is altered in human brain tissue, we fractionated putamen samples of patients with PD and controls (Figures 1A and 1B). We found that levels of synaptosomal HSP10 were reduced in samples from patients. In contrast, the levels of HSP60, the protein partner of HSP10 in the mitochondrial folding complex, and the levels of soluble aSyn were not altered. In parallel, the levels of synaptosomal SOD2 were also reduced in PD brains. Although we found no change in the levels of soluble aSyn in striatal synaptosomes, we detected the colocalization of HSP10 and phospho-aSyn (paSyn) in post-mortem tissue (putamen) from PD patients and from patients with dementia with LBs (DLBs) but not from control brains (Figure 1C; Figure S1). We could also co-immunoprecipitate HSP10 and aSyn from striatal synaptosomal samples of WT or aSyn transgenic mice (Figure 1D). In addition, we found colocalization of HSP10 and aSyn in primary cortical neurons using a proximity ligation assay (PLA; Figure S2). To further validate these results, we used surface plasmon resonance (SPR), a technique that enables estimation of the kinetics and binding constants for protein-protein interactions. We confirmed a high-affinity interaction between HSP10 and monomeric, oligomeric, and pre-formed fibrils (PFFs) of aSyn (Figure 1E). Interestingly, we found that monomeric and PFFs of aSyn showed similar binding affinities to HSP10 (monomeric: K_D = 2.9 μM, k_a = 11.92 M^{-1} s^{-1}, k_d = 3.46 × 10^{-5} s^{-1}; PFF: K_D = 5.27 μM, k_a = 11.00 M^{-1} s^{-1}, k_d = 5.95 × 10^{-5} s^{-1}) and that oligomeric aSyn had lower affinity to HSP10 (K_D = 27.2 μM, k_a = 6.8 M^{-1} s^{-1}, k_d = 1.85 × 10^{-4} s^{-1}).

The Subcellular Distribution of HSP10 Is Altered in Middle-Age aSyn Transgenic Mice

Next, we assessed the levels of HSP10 in striatal synaptosomal mitochondria of aSyn transgenic and control mice (Figure 2). The levels of mitochondrial HSP10 were reduced in both young and middle-age transgenic animals (Figures 2A–2D), but the levels of total striatal HSP10 were not altered either by genotype or by age (Figure 2F). In parallel, the levels of cytosolic HSP10 were increased in both young and middle-age A30PaSyn mice (Figure 2E). To unequivocally confirm the identity and integrity of HSP10, we used a parallel gel electrophoresis approach and subjected the gel band corresponding to immunodetected HSP10 to in-gel protein digestion followed by mass spectrometric protein identification (Ott et al., 2015). Both mitochondrial and cytosolic HSP10 were identified with the same high sequence coverage (Figures 2G and 2H).

Because the HSP60/HSP10 complex is an important player in mitochondrial folding, we next asked whether there were functional consequences of the age-associated decreased levels of mitochondrial HSP10. To better distinguish between synaptic and general effects, we fractionated striatal samples, prepared from young or middle-age animals, into synaptosome and total mitochondrial fractions (Figure S3A). We found reduced spare respiratory capacity (SRC; a measure of mitochondrial function) in synaptosomes prepared from young aSyn transgenic animals (Figure S3B) but not in total mitochondria fractions (Figure S3C). In middle-age transgenic mice, both synaptosomal (Figure S3D) and total mitochondrial SRC (Figure S3E) decreased compared with control animals. In addition, we found that mitochondrial ROS handling (Figure S3F), mitochondrial membrane potential (Figure S3G), and the opening of the mitochondrial permeability transition pore (mPTP; Figure S3H) were also compromised selectively in the striatal synaptic compartment but not in total mitochondrial fractions (Figures S3I and S3J).

HSP10 Improves Mitochondrial Functions in Primary Neuronal Cultures

Because we found reduced levels of mitochondrial HSP10 in the brains of both PD patients and aSyn transgenic animals, we hypothesized that this might be associated with the functional deficits observed in mitochondria. Therefore, we next tested

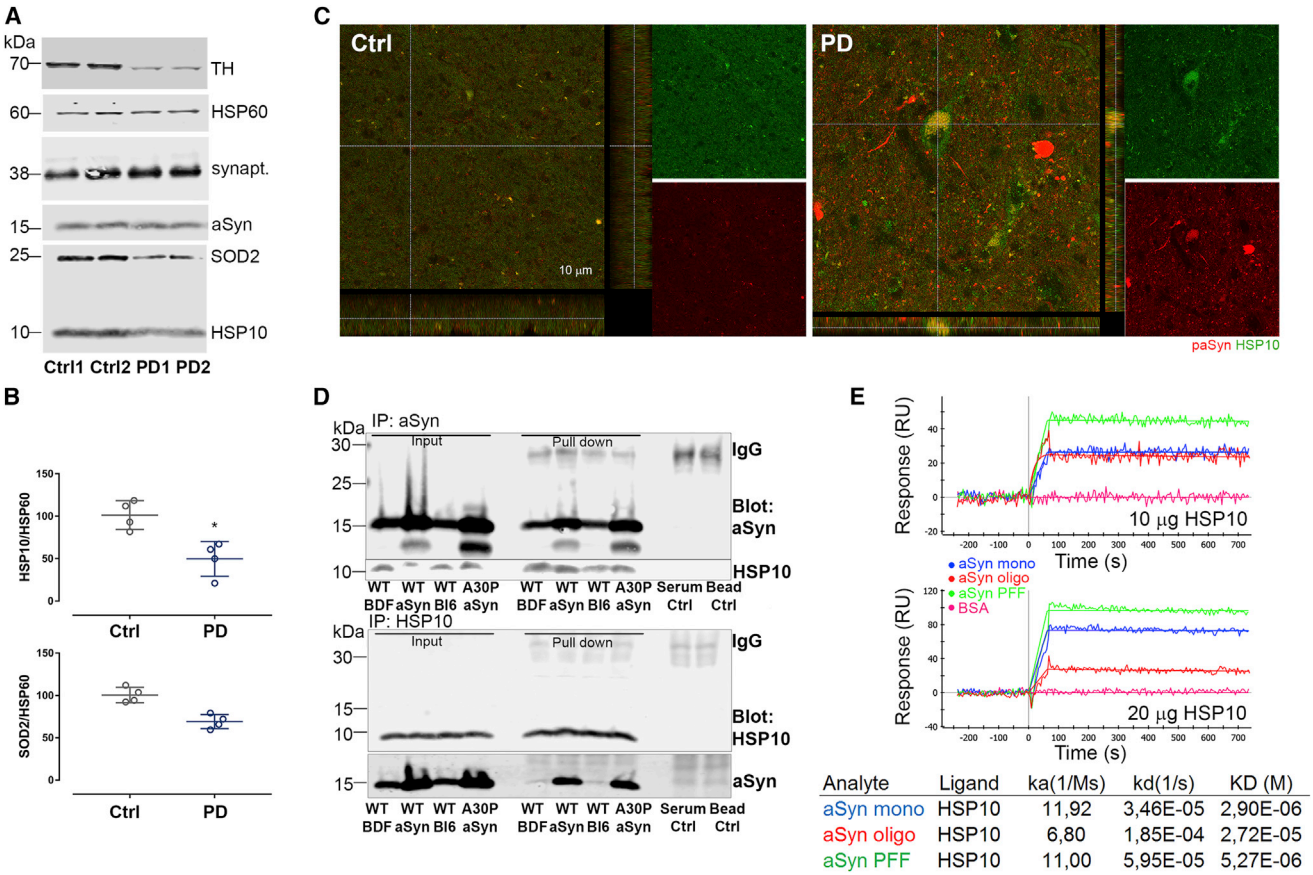

Analyte	Ligand	ka(1/Ms)	kd(1/s)	KD (M)
aSyn mono	HSP10	11,92	3,46E-05	2,90E-06
aSyn oligo	HSP10	6,80	1,85E-04	2,72E-05
aSyn PFF	HSP10	11,00	5,95E-05	5,27E-06

Figure 1. aSyn Interacts with HSP10 in Striatal Synaptosomes and in Human Brain

(A) Synaptosome fractions from the putamen of patients with PD and age-matched controls (Ctrl) (n = 4 per group) were probed for the dopaminergic marker TH, mitochondrial SOD2, synaptic marker synaptophysin (synapt.), aSyn, HSP10, and HSP60.

(B) Quantification of the HSP10/HSP60 and SOD2/HSP60 ratios in PD and control putamen.

(C) Representative confocal microscopy images of the putamen of a control and a PD patient show paSyn (red) staining and colocalization (orange) of paSyn and HSP10 (green). Scale bar: 10 µm.

(D) Representative immunoblot of three independent experiments showing input samples and immunoprecipitation (pull-down) of aSyn (upper blots) or HSP10 (lower blots). Membranes were immunoblotted with anti-aSyn and anti-HSP10 antibodies. Mouse serum and immunobeads were used as negative controls (serum Ctrl and Bead Ctrl, respectively).

(E) Surface plasmon resonance shows high-affinity binding of HSP10 to monomeric and PFF aSyn. aSyn was perfused for 1 min on sensor surfaces on which HSP10 (10 and 20 µg/mL, upper and lower graphs, respectively) had been attached. The nonspecific binding was subtracted. Sensorgrams show the time course of the HSP10-dependent SPR signal in resonance units (RU). Binding parameters are shown in the table below the graph.

Data are presented as mean ± SD. *p < 0.05. PD, Parkinson's disease patient; mono, monomers; oligo, oligomers; PFFs, pre-formed fibrils.

whether increasing the levels of HSP10 would ameliorate aSyn-associated mitochondrial dysfunction. First, we generated an *in vitro* model of synucleinopathies in primary striatal cultures, in which moderate overexpression of aSyn resulted in mild mitochondrial dysfunction. Neurons were infected with lentivirus encoding human WTaSyn, A30PaSyn, or GFP, as control protein. To test whether expression of HSP10 would modify aSyn-induced mitochondrial dysfunction, neuronal cultures were infected with lentivirus encoding for Flag-tagged HSP10 (HSP10-Flag) or GFP. Therefore, we generated six experimental groups: GFP+GFP, GFP+HSP10, WTaSyn+GFP, WTaSyn+HSP-10, A30PaSyn+GFP, and A30PaSyn+HSP10.

We found that expression of human aSyn resulted in a ~30% increase in the total levels (both rodent and human) of aSyn compared with control cells (GFP+GFP versus WTaSyn+GFP or A30PaSyn+GFP) (Figures 3A and 3B; Figure S4A). Expression of human aSyn reduced the levels of endogenous HSP10 just moderately (Figure S4B) but did not affect the levels of HSP60 (Figure 3B; Figure S4C). Expression of human aSyn increased ER stress (elevated levels of growth arrest and DNA damage 153 [GADD153]) (Figures S4D and S4E) and reduced the levels of the mitochondrial serine protease high temperature-regulated A2 (HtrA2) (Figure S4F) and SOD2 (Figures 3B and 3C). mPTPs were more open in cells expressing A30PaSyn (Figure S4G). Interestingly, although basal mitochondrial ROS levels were not increased (Figure S4H), removal of mitochondrial ROS was less efficient in H_2O_2-treated cells (Figure 3D) when human aSyn was expressed. In contrast, basal cytoplasmic ROS levels

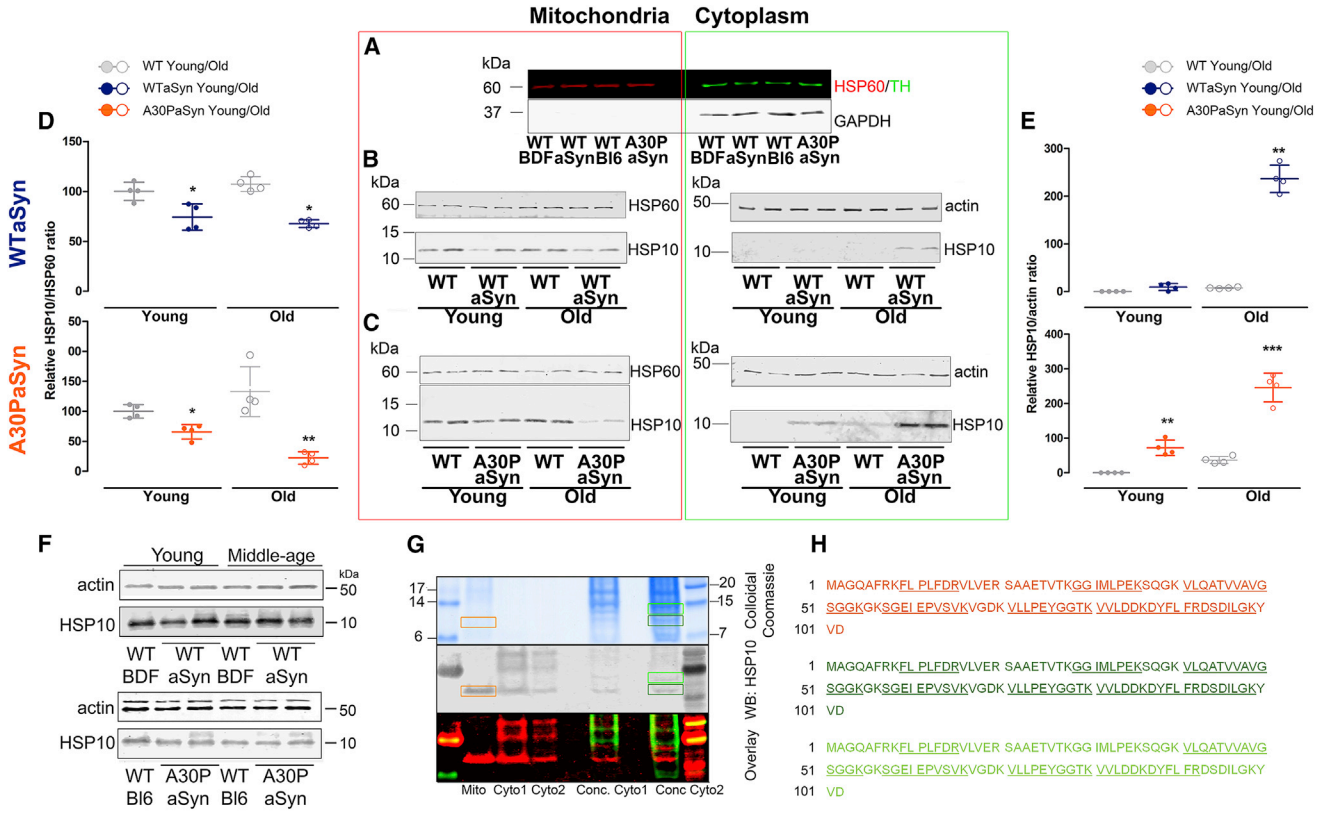

Figure 2. HSP10 Re-localizes from the Mitochondria into the Cytosol of Middle-Age aSyn Transgenic Mice

(A) Representative immunoblot image showing the levels of the mitochondrial marker HSP60 (red) and the cytoplasmic markers TH (green) and GAPDH in the mitochondrial or cytoplasmic fractions prepared from striatal samples.

(B) Immunoblot images show mitochondrial (left) and cytoplasmic (right) HSP10 levels in young and old, control (WT), and WTaSyn transgenic mice.

(C) Immunoblot images show mitochondrial (left) and cytoplasmic (right) HSP10 levels in young and old, control (WT), and A30PaSyn transgenic mice. Mitochondrial levels of HSP10 decreased in both young and middle-age WTaSyn (upper left) and A30PySyn (lower left) mice. In contrast, cytoplasmic levels of HSP10 increased with age in transgenic mice (in WTaSyn mice, it was detectable just in middle-age animals; upper right panel). In A30PaSyn mice, the levels of cytoplasmic HSP10 were increased already in younger animals (lower right) and were further increased with age.

(D) Quantification of the mitochondrial HSP10 levels of WTaSyn and control (upper panel) and A30PaSyn and its control (lower panel) shows reduced protein signal in both young and old transgenic animals.

(E) Quantification of cytoplasmic HSP10 signal shows increased level of HSP10 in aged WTaSyn mice, and in both young and old A30PaSyn mice, compared with control.

(F) Representative immunoblots showing the total level of HSP10 in WT and aSyn transgenic mice. No differences in the total levels of HSP10 were found.

(G) Colloidal Coomassie staining (upper image), HSP10 immunoblot (middle image), and pseudo-colored overlay (lower image) of the same protein lysates. The overlay was used to determine the region to be excised from the Coomassie gel for subsequent MS protein identification (areas indicated by rectangles). Mito, mitochondria sample; Cyto, cytoplasmic sample; conc Cyto, concentrated cytoplasmic sample.

(H) In the amino acid sequence of HSP10 (UniProtKB/Swiss-Prot Q64433), peptides identified by MS are underlined (orange, peptides identified from the mitochondrial fraction; dark green, peptides identified from the cytoplasmic fraction, major lower band; light green, peptides identified from the cytoplasmic fraction, minor upper band).

Data are presented as mean ± SD. *p < 0.05.

were higher (Figure S4I), but H_2O_2-induced ROS elimination was identical in GFP-expressing and in human aSyn-expressing cells (Figure S4J). Expression of both WTaSyn and A30PaSyn significantly reduced the SRC of striatal neurons, with a greater decrease in the A30PaSyn-expressing cultures (Figures 3E and 3F).

Expression of HSP10-Flag resulted in a ~2-fold increase in the total levels of HSP10 protein (GFP+HSP10, WTaSyn+HSP10, and A30PaSyn+HSP10; Figure 3B; Figure S4B). In WTaSyn-expressing cells, overexpression of HSP10 resulted in increased SOD2 levels (Figures 3B and 3C), and consequently, removal of mitochondrial ROS upon H_2O_2 treatment was improved (Figure 3D). In addition, the mitochondrial HtrA2 levels (Figures S4D and S4F) and SRC (Figures 3E and 3F) were both normalized. In contrast, although basal cytoplasmic ROS decreased in cells co-expressing WTaSyn and HSP10 (Figure S4I), ER stress levels were not changed (Figures S4D and S4E).

Overexpression of HSP10 in A30PaSyn-infected cells improved the elimination of mitochondrial ROS after oxidative

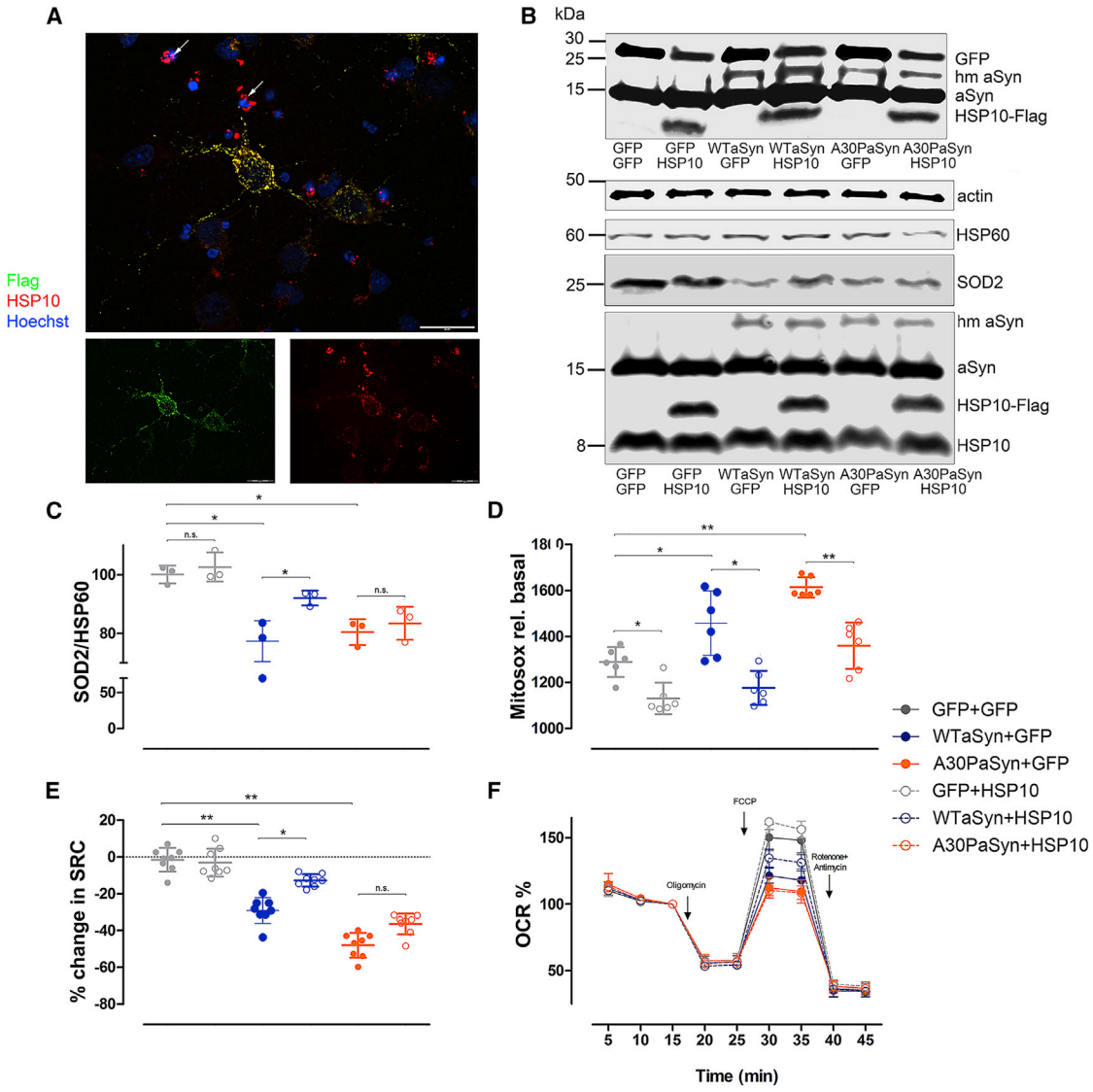

Figure 3. Hsp10 Mitigates Mitochondrial Dysfunction in Primary Neurons Expressing Human WTaSyn

(A) Immunofluorescence images of primary neurons stained for HSP10-Flag (green) and HSP10 (red) showing colocalization (yellow). HSP10-Flag is not expressed in glial cells (arrows). Scale bar: 20 μm.

(B) Representative immunoblots of three independent experiments showing the levels of HSP10, HSP10-Flag, GFP, and endogenous and human aSyn (human aSyn with T2A tag [molecular weight (MW) ~1.3 kDa higher than that of endogenous rat aSyn; Tang et al., 2009) in primary neurons. The levels of endogenous aSyn and HSP60 are not changed, while the levels of SOD2 decreases with human aSyn expression (n = 3). Quantifications of aSyn, HSP10, and HSP60 are shown in Figures S5A–S5D).

(C) Quantification of SOD2 protein levels in primary cultures. Levels of SOD2 decrease in cells expressing WT or A30P aSyn, and increased HSP10 expression improves only WTaSyn-induced SOD2 protein loss.

(D) Expression of human WTaSyn or A30PaSyn reduced mitochondrial ROS handling, while expression of HSP10 improved ROS handling in cells expressing human aSyn and in control cells expressing GFP, but not in cells expressing A30PaSyn (n = 3).

(E and F) Primary neuronal cultures expressing human aSyn displayed reduced SRC (n = 8). HSP10 improved SRC in cells expressing WTaSyn but not in cells expressing A30PaSyn.

(E) Graph displaying the changes in the SRC in response to various treatments, normalized to control cultures.

(F) Mitochondrial respiration of the various cultures measured by OCR levels under basal conditions (measurement at 5 and 10 min) or following the addition of oligomycin, the uncoupler FCCP, or rotenone and antimycin. SRC was quantified by normalization of OCR levels to the total numbers of cells.

Data are presented as mean ± SD. *p < 0.05.

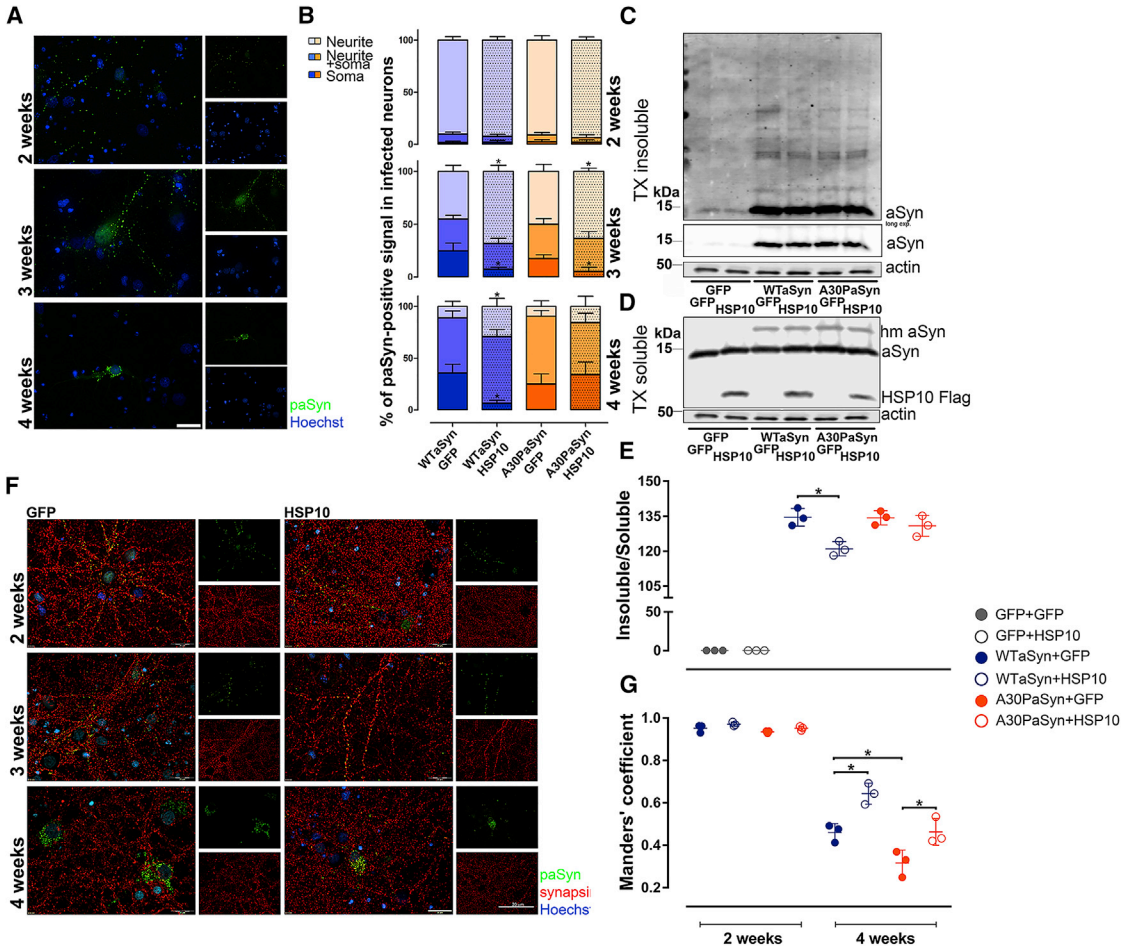

Figure 4. HSP10 Delays aSyn Pathology in Primary Neuronal Cultures

(A) Microscopy images (representative of three independent experiments) showing the localization of paSyn (green) in primary neurons overexpressing human WTaSyn 2 or 4 weeks after viral vector transduction. Scale bar: 20 μm.

(B) Localization of paSyn-positive signal was quantified in cultures after 2, 3, or 4 weeks of aSyn expression. paSyn signal was classified as neuritic (neurite), when signal was present just in the neurites of a single neuron; juxtacellular (soma), when signal was present just in the perinuclear area; or mixed (neurite + soma), when both neuritic and juxtacellular signal was observed.

(C–E) aSyn solubility in Triton X-100 increased in cultures infected with HSP10.

(C) Representative immunoblot shows aSyn in the Triton X-100 (TX) insoluble fraction.

(D) The levels of aSyn did not change in the Triton X-100 soluble fraction (lysates from the same preparation, as in (C).

(E) Ratio of Triton X-100 insoluble and soluble aSyn decreases in "old" cultures when HSP10 is expressed (n = 3).

(F) Microscopy images (representative images of three independent experiments) showing the colocalization of paSyn (green) and synapsin (red) in primary neuronal cultures expressing WTaSyn and HSP10 or GFP, as a control, 2, 3, or 4 weeks of aSyn expression. Scale bar: 20 μm.

(G) Colocalization was assessed by Mander's overlap coefficient using ImageJ JACoP plugin after 2 or 4 weeks of aSyn expression. Almost complete colocalization was observed in young cultures (Mander's coefficient ~0.95), indicating the presynaptic presence of paSyn. In old cultures, colocalization of paSyn and synapsin was lower (Mander's coefficient ~0.46 ± 0.04 for WTaSyn and 0.32 ± 0.06 for A30PaSyn) but remained higher in cultures expressing HSP10 (0.64 ± 0.05 for WTaSyn and 0.46 ± 0.07 for A30PaSyn).

Data are presented as mean ± SD. *p < 0.05.

stress (Figure 3D) but did not alter the levels of SOD2 or HtrA2. Similarly, SRC was not improved upon HSP10 overexpression (Figures 3E and 3F).

HSP10 Reduces aSyn Pathology

The aggregation of aSyn is enhanced in oxidative environments (Hashimoto et al., 1999; Fernandes et al., 2014; Scudamore and Ciossek, 2018). Because increasing the levels of HSP10 improved mitochondrial ROS handling and decreased basal cytoplasmic ROS levels, we next tested whether HSP10 overexpression modulated aSyn aggregation. We compared the levels of aSyn phosphorylation on S129 (paSyn, used as a readout of aSyn pathology) in neurons expressing WTaSyn or A30PaSyn together with either HSP10 or GFP (see the six groups above) (Oueslati, 2016). After 2 weeks in culture, paSyn was found mostly in puncta along the neurites (Figures 4A and 4B) and

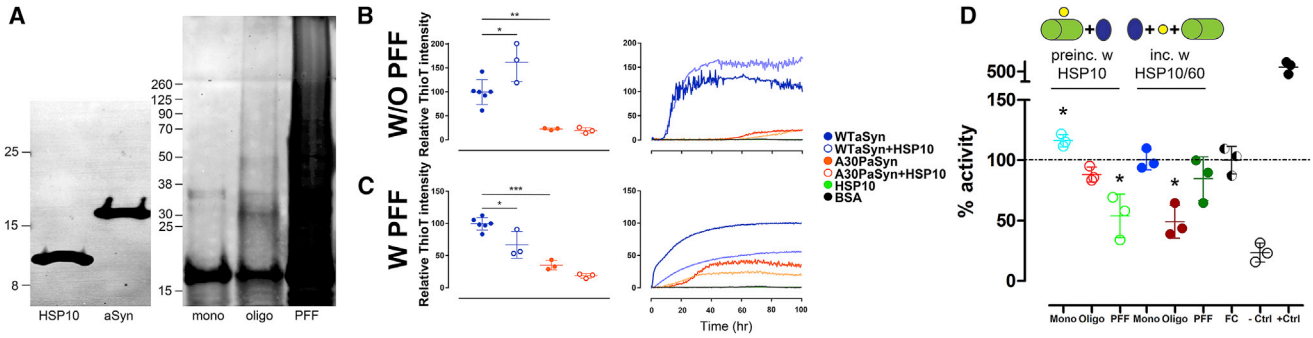

Figure 5. HSP10 Reduces aSyn Aggregation *In Vitro*

(A) Representative SDS-PAGE image of the recombinant proteins used for further experiments. Protein identity was confirmed by mass spectrometry analyses. Left blot: 0.1 μg HSP10 and 0.1 μg monomeric aSyn were loaded on the gel. Right blot: 0.05 μg monomeric and 0.1 μg oligomeric or PFF aSyn were loaded on a native gel.

(B) Quantification of the results of the RT-QuiC experiment shows that HSP10 (1/10 of the amount of aSyn) increases the aggregation of WTaSyn from the monomers, while A30PaSyn aggregation was not affected by HSP10.

(C) When aSyn PFF seeds are present, HSP10 reduces WTaSyn aggregation. Left panels in (B) and (C): quantification of the relative ThioT fluorescence signal after the last cycle of the RT-QuIC assay. Right panels in (B) and (C): representative curves showing the fluorescent signal over time.

(D) Folding activity of the HSP60/HSP10 complex after pre-incubation of HSP10 with 100 nM monomeric, oligomeric, or PFFs of aSyn ("pre-incubation") or after incubation of different aSyn species together with HSP10 and HSP60 ("incubation"). FC, folding control; the complex was incubated with BSA instead of aSyn; −Ctrl, folding activity without addition of ATP; +Ctrl, activity in the presence of the folding client without heat shock.

Data are presented as mean ± SD. *$p < 0.05$.

colocalized almost completely with synapsin (Figures 4F and 4G) in all cultures expressing human aSyn. Two weeks later, most neurons expressing human aSyn + GFP displayed paSyn in the soma, and the colocalization of paSyn and synapsin was reduced. Interestingly, HSP10 delayed the re-localization of paSyn-positive puncta from the neurites toward the soma, and the colocalization with synapsin remained relatively high even after 4 weeks in culture (Figures 4B and 4G).

To further confirm the modulation of aSyn aggregation by HSP10, we assessed the solubility of aSyn in Triton X-100 in the older cultures (Figures 3C–3E). We found that the ratio of insoluble to soluble aSyn decreased in primary cells expressing WTaSyn+HSP10 compared with cells expressing WTaSyn+GFP. However, HSP10 expression had no effect in A30PaSyn-expressing cells (Figures 4C–4E).

Next, we assessed the conversion of monomeric aSyn into fibrils *in vitro*, using the real-time quaking-induced conversion (RT-QuIC) assay (Candelise et al., 2019; van Rumund et al., 2019). Briefly, WTaSyn or A30PaSyn monomers were incubated in the presence or absence of HSP10, and the aggregation was monitored by measuring thioflavin T fluorescence. Alternatively, WTaSyn or A30PaSyn monomers were seeded with PFFs of WTaSyn in the presence of HSP10. Only freshly thawed aSyn monomers were used, and the quality of the preparations was assessed using immunoblot (Figure 5A). WTaSyn monomers aggregated even without PFF seeding (Figure 5B) and HSP10 increased aggregation. Interestingly, in the presence of PFF seeds, HSP10 decreased aSyn aggregation (Figure 5C). In contrast, A30PaSyn monomers formed almost no thioflavin T-positive species without PFF seeding, irrespective of the presence of HSP10 (Figure 5B). Although the presence of PFF seeds increased A30PaSyn aggregation, HSP10 had no effect (Figure 5C).

aSyn Affects HSP10/HSP60 Folding Activity

Because we found increased levels of cytoplasmic HSP10 in middle-age transgenic mice, we hypothesized that cytosolic aSyn might bind to and, therefore, sequester HSP10 in the cytoplasm, reducing the amount of protein that would normally localize in mitochondria. As a corollary of this hypothesis, this should result in reduced folding capacity of the HSP60/HSP10 complex. To test this, we used two distinct approaches. One mimicked a situation in which different aSyn species (monomers, oligomers, and PFFs) would interact with Hsp10 in the cytosol (Figure 5D, pre-incubation with HSP10). The other mimicked a situation in which the different aSyn species would interact with the HSP60/HSP10 complex in mitochondria (Figure 5D, incubation with HSP10 and HSP60). Interestingly, while aSyn monomers increased the folding activity when pre-incubated with HSP10 (before adding HSP60), incubation of aSyn together with HSP10 and HSP60 did not change complex activity. Oligomeric aSyn species reduced the folding activity only when added together with HSP10 and HSP60. In contrast, aSyn PFFs pre-incubated with HSP10 significantly reduced the folding activity of the complex but had no effect when incubated together with HSP10 and HSP60 (Figure 5D). These findings suggest conformation-specific interactions between aSyn and HSP10, consistent with the SPR data, and suggest that aggregated aSyn in the cytosol impairs the activity of the HSP10/HSP60 complex.

HSP10 Improves Mitochondrial Function *In Vivo*

Next, to determine whether we could rescue aSyn-associated pathologies *in vivo*, we injected lentiviruses encoding either HSP10 or GFP in the SN of WT or aSyn transgenic mice. HSP10 and GFP were detected both in synaptosomes prepared from the striatum and in dopaminergic neurons of the SN (Figures 6A and 6D). One month after viral injection, neither the number of tyrosine hydroxylase (TH)-positive (dopaminergic)

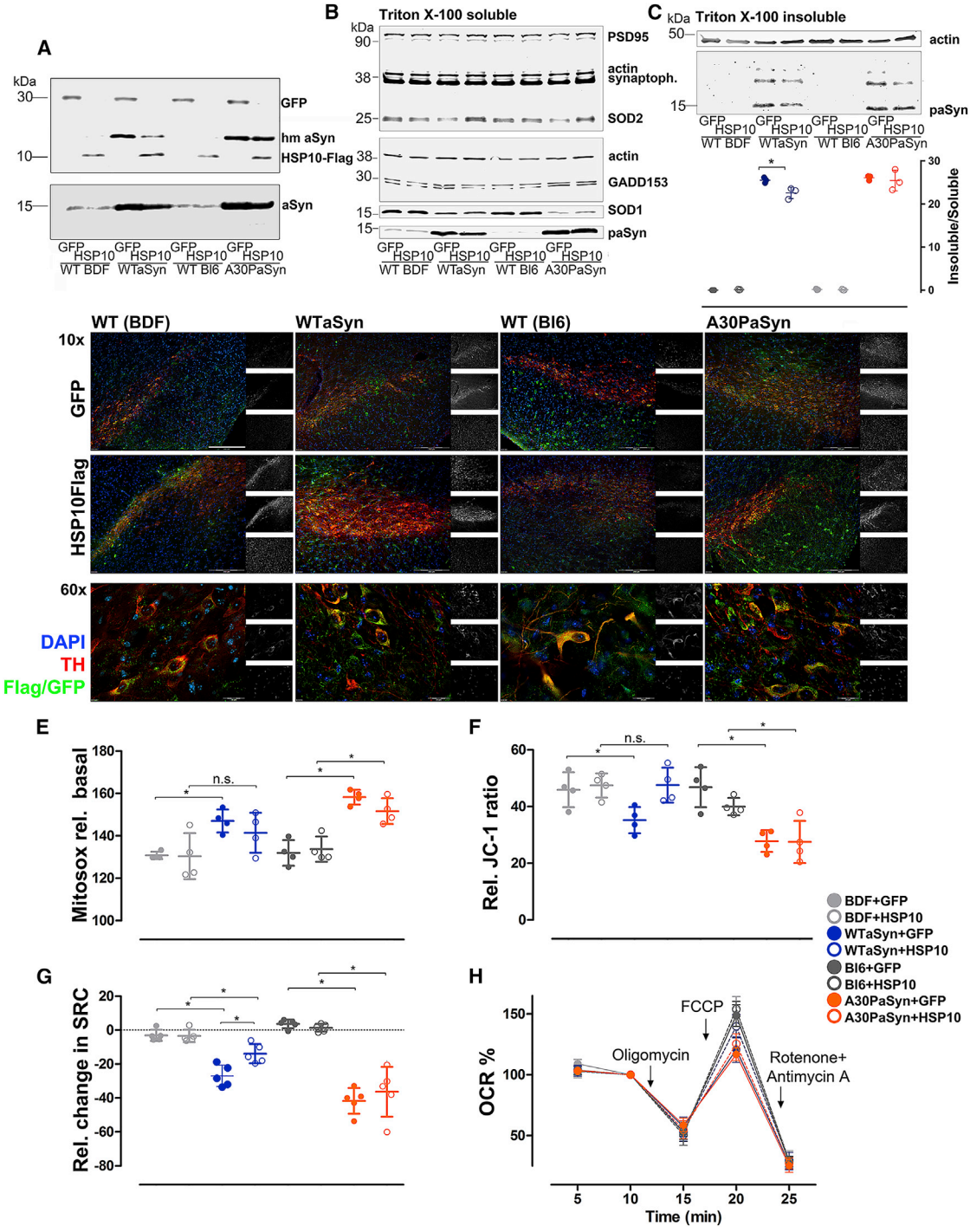

Figure 6. Viral Vector-Mediated Overexpression of HSP10 in the Substantia Nigra Restores aSyn-Induced Mitochondrial Dysfunction and Reduces ER Stress in Striatal Synaptosomes

(A) Representative immunoblot showing the levels of human aSyn, HSP10-Flag, and GFP in striatal synaptosomes of WT control or transgenic mice infected with HSP10-Flag or GFP encoding viruses in the SN.

(B and C) Representative immunoblots showing the striatal levels of the post-synaptic density protein PSD95, presynaptic synaptophysin, SOD1, SOD2, GADD153, and paSyn in the Triton X-100 soluble fraction (B), or the striatal levels of paSyn in the Triton X-100 insoluble fraction, and quantification of ratio of soluble to insoluble aSyn (C) after the intranigral injection of lentiviruses encoding GFP or HSP10-Flag. Symbols are in (E)–(H). Quantification of the relative levels of GADD153, SOD1, and SOD2 is shown in Figures S5C–S5E (n = 3).

(legend continued on next page)

neurons nor the total number of neurons (Nissl) changed compared with control mice (Figures S5A and S5B). We found no alterations in the levels of synaptophysin or PSD95 in striatal synaptosomes (Figure 6B). ER stress (GADD153) was increased, and SOD1 and SOD2 levels were decreased in transgenic mice (Figure 6C). Expression of HSP10 did not change the levels of SOD1. In contrast, it decreased the levels of GADD153 in WTaSyn transgenic animals (Figure 6B). The levels of synaptosomal SOD2, a protein folded by the HSP60/HSP10 complex, was restored to control levels upon overexpression of HSP10 (Figure 6B). Interestingly, increased striatal HSP10 also reduced aSyn aggregation in synaptosomes of WTaSyn transgenic mice, as assessed using Triton X-100 solubility (Figure 6C).

Next, we hypothesized that the restoration of SOD2 levels in HSP10-injected animals might reduce mitochondrial ROS levels and/or improve ROS handling. Although basal mitochondrial ROS levels were not altered by HSP10 overexpression, the handling of ROS upon H_2O_2 stress improved in HSP10-injected WTaSyn transgenic mice and was identical to that observed in control animals (Figures 6E and S5F–S5H).

Because the folding and import of several mitochondrial proteins, including components of the respiratory chain, are mediated by the HSP60/HSP10 complex (Tang et al., 2016), we next tested whether HSP10 would also restore mitochondrial SRC. We found that HSP10 significantly increased SRC in striatal synaptosomes prepared from WTaSyn animals but not from A30PaSyn mice (Figures 6G and 6H).

DISCUSSION

Consistent with the occurrence of functional synaptic alterations in early, preclinical stages of synucleinopathies, we discovered that in the nigrostriatal system, aSyn-induced synaptic mitochondrial pathology starts prior to the total mitochondrial pathology. We report that aSyn interacts with HSP10 in the striatal synaptic compartment and that this interaction results in the sequestration of HSP10 in the cytosol in conditions of increased aSyn load, leading to the impairment of several mitochondrial functions. We hypothesized that this happens because when HSP10 is sequestered in the cytosol, the normal folding of client proteins of the mitochondrial HSP10/HSP60 complex is compromised. By increasing the levels of HSP10, we improved aSyn-associated mitochondrial dysfunction and delayed aSyn pathology.

When levels of aSyn are increased, because of age-associated changes in its turnover or because of the effect of PTMs (de Oliveira et al., 2017; Vicente Miranda et al., 2017), aSyn may gain toxic properties and associate with mitochondria. Consistently, overexpression of aSyn or treatment of cells with aSyn oligomers or fibrils also induces severe mitochondrial deficits, including fragmentation (Nakamura et al., 2011), mitophagy (Chinta et al., 2010), and impaired mitochondrial protein import (Di Maio et al., 2016). However, the precise effect of aSyn on mitochondrial function is still controversial. Although some studies show no effect of aSyn in dopaminergic nerve terminals (Pathak et al., 2017), others have reported protection even against the mitochondrial toxin MPP^+ (Dauer et al., 2002; Fountaine and Wade-Martins, 2007).

To gain insight into the initial effects of aSyn in nerve terminals, we searched for aSyn interactors in striatal synaptosomes. Among several other candidates, we identified HSP10 as a novel aSyn-interacting protein and asked whether manipulating the levels of this small heat shock protein could reverse aSyn-associated cellular pathologies. HSP10 is encoded by a nuclear gene (*HSPE1*, 2q33.1), arranged head to head with the gene encoding HSP60 and controlled by the same bi-directional promoter (Hansen et al., 2003). In mitochondria, HSP10 assembles into either an asymmetric (one HSP10 heptameric ring) or a symmetric (two rings) complex with an HSP60 14-mer. Interestingly, the levels of HSP10 limit the formation of the symmetric complexes, and the asymmetric complex has reduced folding capacity (Nisemblat et al., 2015). Because the HSP10/HSP60 complex is one of the most important players in mitochondrial quality control (Horwich et al., 2007; Campos et al., 2016), reduced function of the complex results in embryonic lethality (Christensen et al., 2010), and a heterozygous mutation in the *HSPE1* gene associates with severe, early-onset neurological disorder in humans (Bie et al., 2016). Although the mutant protein is functional, its resistance to proteases is substantially reduced, resulting in an almost 2-fold reduction in the HSP10/HSP60 ratio. Because decreased HSP10 concentration forces the formation of the asymmetric, less efficient, folding complex, the levels of client proteins, such as SOD2, are reduced to just 20% of the normal levels, and mitochondrial ROS levels are increased (Azem et al., 1995). Our finding that, in parallel with reduced mitochondrial HSP10 levels in striatal synaptosomes, both mitochondrial ROS removal and SOD2 level are decreased, suggests that HSP10 may play a central role in aSyn-associated mitochondrial dysfunction in synucleinopathies. Although in our model, the levels of other mitochondrial proteins (e.g., TOM20, HSP60, frataxin; data not shown) were not altered, we cannot rule out that aSyn alters mitochondrial protein import through another mechanism. Our results also suggest that the A30P mutation in aSyn may potentiate the interaction between aSyn and HSP10, leading to an earlier decrease in mitochondrial HSP10 levels and mitochondrial dysfunction.

(D) Representative microscopy images of the SN of wild-type (WT BDF or WT Bl6) and transgenic (WTaSyn or A30PaSyn) mice after injection of GFP as control or HSP10-Flag encoding virus. Scale bar: 200 μm (10×) or 20 μm (60×). Thirty micrometer coronal section containing the SN where the virus injection was visible was stained with anti-tyrosine hydroxylase antibody (TH; red) to detect dopaminergic neurons, anti-GFP or anti-Flag antibody (green) to detect the expression of exogenous protein, and DAPI (blue).

(E) Mitochondrial ROS handling in striatal synaptosomes improved in WTaSyn mice upon HSP10 overexpression (n = 4).

(F) The FCCP-induced depolarization in striatal synaptosomes of WTaSyn mice, but not in A30PaSyn mice, was reduced upon HSP10 overexpression (n = 4).

(G) Change in SRC in striatal synaptosomes normalized to preparations from WT control animals (n = 5).

(H) Mitochondrial respiration measured by relative OCR levels in striatal synaptosomes, under basal conditions (measurement at 5 and 10 min) or following the addition of oligomycin (15 min), the uncoupler FCCP (20 min), or rotenone and antimycin (25 min).

Data are presented as mean ± SD. *$p < 0.05$.

Given that HSP10 is synthetized in the cytosol, and that aSyn is also primarily a cytosolic protein, we hypothesized that the main site for the interaction between the two proteins would be the cytosol. We predicted that increased levels of aSyn would bind more HSP10 and, consequently, reduce its mitochondrial levels and activity, thereby leading to the impairment of mitochondrial quality control and respiration at synapses. We also hypothesized that as a chaperone, HSP10 might affect aSyn aggregation. We tested both hypotheses and assessed (1) HSP60/HSP10 folding activity in the presence of different aSyn species and (2) the aggregation of aSyn in the presence of HSP10. We found that aggregated forms of aSyn (PFFs) did not change the folding activity of the already formed HSP10/HSP60 complex per se. However, pre-incubation of PFFs with HSP10, to mimic the interaction between aSyn and HSP10 in the cytosol, reduced the folding activity of the complex by approximately 50%. Because under pathological conditions aSyn accumulates and aggregates in the cytosol, where newly synthetized, non-complexed HSP10 is also present, our data suggest that certain aggregated forms of aSyn interact with HSP10 in the cytosol, prevent its import into mitochondria, and thereby reduce the activity of the HSP60/HSP10 complex. This is supported by the SPR data showing that aSyn monomers and PFFs interact with HSP10 with high affinity. In comparison, the dissociation constants obtained in the SPR experiment were identical to those described for aSyn and S100A9 interaction (Horvath et al., 2018). In addition, we found a significant fraction of HSP10 in the cytoplasm, alongside decreased levels of mitochondrial HSP10.

We also found that HSP10 influenced the aggregation of aSyn. Although monomeric aSyn aggregated faster in the presence of HSP10, the aggregation was slower when both aSyn PFF and HSP10 were present. These results suggest that aSyn aggregation may start at lower concentrations when HSP10 is present and that once aSyn seeds are formed, the aggregation process is slowed down by HSP10. The aggregation properties of A30P aSyn species were not altered by HSP10. Because the effects of A30P aSyn on mitochondria appeared to be stronger than those observed with WT aSyn, and increasing the levels of HSP10 did not improve aSyn pathology or mitochondrial dysfunction, one might speculate that A30P aSyn oligomeric or monomeric species trap HSP10 and induce pathology. Further investigations in future will be necessary to clarify the significance of these findings.

The connection between aSyn pathology and mitochondrial dysfunction in PD is complex. Dysfunctional mitochondria produce less ATP and more ROS, and because of the high energy demand in the synaptic compartment, lowering ATP leads to synaptic dysfunction (Rangaraju et al. 2014) and triggers aSyn accumulation (Nakata et al., 2012). In addition, mitochondrial health correlates with axonal transport, regeneration (Smith and Gallo, 2018), and, consequently, the clearance of aSyn (Oh et al., 2017). Similarly, increased ROS levels facilitate aSyn aggregation (Tabner et al., 2006; Fernandes et al., 2014). This suggests that improving mitochondrial health might also contribute to a reduction in the levels of pathological species of aSyn. Other chaperones, such as HSP27 (Outeiro et al., 2006; Cox et al., 2018), HSP70 (Outeiro et al., 2008; Gao et al., 2015; Aprile et al., 2017), and HSP90 (Du et al., 2014; Xiong et al., 2015), have already been shown to modulate aSyn aggregation and toxicity. However, in our model, we found no evidence for aSyn-associated changes in the levels of these chaperones. We found that the levels of HSP10 were reduced upon aSyn overexpression and that overexpressing HSP10 mitigated most mitotoxic effects of WT aSyn but not of A30P aSyn. Importantly, expression of HSP10 in the SN of WT aSyn mice, but not A30P aSyn mice, improved mitochondrial respiration and ROS handling in striatal synapses, consistent with the effects observed in synaptic terminals.

In general, we found that A30P aSyn induced stronger cellular pathologies compared with WTaSyn. Our data suggest that the differences between WT and A30P aSyn might be because of the mutation, rather than a simple protein load effect, because in our cell culture model the levels of human aSyn were identical (Figure 2B). The levels were also similar in the two transgenic mouse lines used (Figure 4A). A30P mutant aSyn impairs autophagy (Song et al., 2009), which leads to higher ER stress and, ultimately, mitochondrial dysfunction (Ganguly et al., 2018), suggesting also a more downstream, non-HSP10-dependent effect. Consistently, we found that overexpression of HSP10 was less efficient in mitigating those pathologies. The molecular effects of the A30P mutation on aSyn function and toxicity are still unclear. Although a recent study suggests that the A30P mutation induces a loss of function (Pozo Devoto et al., 2017), others support an age-dependent reduction in mitochondrial function (Robson et al., 2018) and increased toxicity (Ysselstein et al., 2017). We have also recently reported different effects on gene expression in both cell and animal models (Paiva et al., 2018; Pinho et al., 2019), and different aggregation propensity (Lázaro et al., 2014), suggesting that multiple effects may contribute to the differences observed.

In conclusion, our study provides novel insight into the molecular mechanisms underlying aSyn-mediated mitochondrial dysfunction in PD and other synucleinopathies and opens novel perspectives for the design of strategies aimed at improving cellular pathologies associated with these devastating diseases.

STAR★METHODS

Detailed methods are provided in the online version of this paper and include the following:

- KEY RESOURCES TABLE
- LEAD CONTACT AND MATERIALS AVAILABILITY
- EXPERIMENTAL MODEL AND SUBJECT DETAILS
  - Ethical statement and animal lines
  - Patients and controls
- METHOD DETAILS
  - Lentivirus injections and tissue dissection
  - Primary neuronal culture
  - Constructs
  - Cell lysis, tissue fractionation, western blotting and immunoprecipitation
  - Mitochondrial assays
  - Recombinant aSyn and HSP10 expression and purification

- HSP10/HSP60 protein refolding assay
- Surface-Plasmon Resonance (SPR) measurements
- aSyn real time quaking-induced conversion (RT-QuiC)
- Proteomic screen of Syn-interacting proteins
- Identification of HSP10 from cytoplasmic fractions by mass spectrometry
- *In situ* Proximity Ligation Assay (PLA)
- Immunostainings, microscopy, and stereology

● QUANTIFICATION AND STATISTICAL ANALYSIS
● DATA AND CODE AVAILABILITY

SUPPLEMENTAL INFORMATION

Supplemental Information can be found online at https://doi.org/10.1016/j.celrep.2019.06.009.

ACKNOWLEDGMENTS

We thank Katharina Grewe and Christine Jünemann for technical assistance, Péter Batáry for assistance with statistical analysis, Ákos Gerencsér for technical advice, and Dr. Andrew C. McCourt for language editing. É.M.S. was supported by the Dorothea Schlözer Program (Georg-August University, Göttingen, Germany), János Bolyai Research Fellowship (Hungarian Academy of Sciences) and ÚNKP Bolyai+ Research Fellowship (Ministry for Innovation and Technology, Hungary). T.F.O. was supported by the DFG Center for Nanoscale Microscopy and Molecular Physiology of the Brain (CNMPB); SFB 1286 (project B8); CAPES/DAAD under the PROBRAL Program; and a grant from Fundación La Marato de TV3 (20144330). A.D.-M. was supported by the Galician Government (Programa de axuda á etapa posdoutoral, XUGA, GAIN, ED481B 2017/053). R.P. was supported by a PhD fellowship from FCT (SFRH/BD/80884/2011). W.L. and J.L. were supported by the National Natural Science Foundation (81430025, 81701265, 31800898, and U801681) and the Swedish Research Council.

AUTHOR CONTRIBUTIONS

É.M.S. designed the study, performed *in vivo* and *in vitro* experiments, analyzed and interpreted data, and wrote the manuscript. E.G. and C.F. did molecular cloning, virus production, and cell culture. R.P. and A.V.-P. performed cell culture. A.K. produced recombinant proteins and prepared the graphical abstract. A.D.-M. performed the RT-QuIC experiment. O.J. did mass spectrometry (MS) analysis. D.J.K., M.J., and J.A. provided human samples and performed human brain staining. S.R. performed electron microscopy (EM). T.T. and M.S. performed SPR analysis. I.Z. analyzed data. T.F.O. obtained funding, designed the study, interpreted data, and wrote the manuscript.

DECLARATION OF INTERESTS

The authors declare no competing interests.

Received: November 23, 2018
Revised: April 19, 2019
Accepted: June 3, 2019
Published: July 2, 2019

REFERENCES

Aprile, F.A., Källstig, E., Limorenko, G., Vendruscolo, M., Ron, D., and Hansen, C. (2017). The molecular chaperones DNAJB6 and Hsp70 cooperate to suppress α-synuclein aggregation. Sci. Rep. *7*, 9039.

Atanassov, I., and Urlaub, H. (2013). Increased proteome coverage by combining PAGE and peptide isoelectric focusing: comparative study of gel-based separation approaches. Proteomics *13*, 2947–2955.

Azem, A., Diamant, S., Kessel, M., Weiss, C., and Goloubinoff, P. (1995). The protein-folding activity of chaperonins correlates with the symmetric GroEL14(-GroES7)2 heterooligomer. Proc. Natl. Acad. Sci. U S A *92*, 12021–12025.

Banerjee, K., Sinha, M., Pham, Cl.L., Jana, S., Chanda, D., Cappai, R., and Chakrabarti, S. (2010). α-synuclein induced membrane depolarization and loss of phosphorylation capacity of isolated rat brain mitochondria: implications in Parkinson's disease. FEBS Lett. *584*, 1571–1576.

Betzer, C., Movius, A.J., Shi, M., Gai, W.P., Zhang, J., and Jensen, P.H. (2015). Identification of synaptosomal proteins binding to monomeric and oligomeric α-synuclein. PLoS ONE *10*, e0116473.

Bie, A.S., Fernandez-Guerra, P., Birkler, R.I., Nisemblat, S., Pelnena, D., Lu, X., Deignan, J.L., Lee, H., Dorrani, N., Corydon, T.J., et al. (2016). Effects of a mutation in the *HSPE1* gene encoding the mitochondrial co-chaperonin HSP10 and its potential association with a neurological and developmental disorder. Front. Mol. Biosci. *3*, 65.

Blin, O., Desnuelle, C., Rascol, O., Borg, M., Peyro Saint Paul, H., Azulay, J.P., Billé, F., Figarella, D., Coulom, F., Pellissier, J.F., et al. (1994). Mitochondrial respiratory failure in skeletal muscle from patients with Parkinson's disease and multiple system atrophy. J. Neurol. Sci. *125*, 95–101.

Bose, A., and Beal, M.F. (2016). Mitochondrial dysfunction in Parkinson's disease. J. Neurochem. *139* (*S1*), 216–231.

Bross, P., and Fernandez-Guerra, P. (2016). Disease-associated mutations in the HSPD1 gene encoding the large subunit of the mitochondrial HSP60/HSP10 chaperonin complex. Front. Mol. Biosci. *3*, 49.

Bross, P., Li, Z., Hansen, J., Hansen, J.J., Nielsen, M.N., Corydon, T.J., Georgopoulos, C., Ang, D., Lundemose, J.B., Niezen-Koning, K., et al. (2007). Single-nucleotide variations in the genes encoding the mitochondrial Hsp60/Hsp10 chaperone system and their disease-causing potential. J. Hum. Genet. *52*, 56–65.

Calì, T., Ottolini, D., Negro, A., and Brini, M. (2012). α-Synuclein controls mitochondrial calcium homeostasis by enhancing endoplasmic reticulum-mitochondria interactions. J. Biol. Chem. *287*, 17914–17929.

Calo, L., Wegrzynowicz, M., Santivañez-Perez, J., and Grazia Spillantini, M. (2016). Synaptic failure and α-synuclein. Mov. Disord. *31*, 169–177.

Campos, J.C., Bozi, L.H., Bechara, L.R., Lima, V.M., and Ferreira, J.C. (2016). Mitochondrial quality control in cardiac diseases. Front. Physiol. *7*, 479.

Candelise, N., Schmitz, M., Llorens, F., Villar-Piqué, A., Cramm, M., Thom, T., da Silva Correia, S.M., da Cunha, J.E.G., Möbius, W., Outeiro, T.F., et al. (2019). Seeding variability of different alpha synuclein strains in synucleinopathies. Ann. Neurol. *85*, 691–703.

Chang, D., Nalls, M.A., Hallgrímsdóttir, I.B., Hunkapiller, J., van der Brug, M., Cai, F., Kerchner, G.A., Ayalon, G., Bingol, B., Sheng, M., et al.; International Parkinson's Disease Genomics Consortium; 23andMe Research Team (2017). A meta-analysis of genome-wide association studies identifies 17 new Parkinson's disease risk loci. Nat. Genet. *49*, 1511–1516.

Chinta, S.J., Mallajosyula, J.K., Rane, A., and Andersen, J.K. (2010). Mitochondrial α-synuclein accumulation impairs complex I function in dopaminergic neurons and results in increased mitophagy in vivo. Neurosci. Lett. *486*, 235–239.

Christensen, J.H., Nielsen, M.N., Hansen, J., Füchtbauer, A., Füchtbauer, E.M., West, M., Corydon, T.J., Gregersen, N., and Bross, P. (2010). Inactivation of the hereditary spastic paraplegia-associated Hspd1 gene encoding the Hsp60 chaperone results in early embryonic lethality in mice. Cell Stress Chaperones *15*, 851–863.

Corti, O., Lesage, S., and Brice, A. (2011). What genetics tells us about the causes and mechanisms of Parkinson's disease. Physiol. Rev. *91*, 1161–1218.

Cox, D., Whiten, D.R., Brown, J.W.P., Horrocks, M.H., San Gil, R., Dobson, C.M., Klenerman, D., van Oijen, A.M., and Ecroyd, H. (2018). The small heat shock protein Hsp27 binds α-synuclein fibrils, preventing elongation and cytotoxicity. J. Biol. Chem. *293*, 4486–4497.

Dauer, W., Kholodilov, N., Vila, M., Trillat, A.C., Goodchild, R., Larsen, K.E., Staal, R., Tieu, K., Schmitz, Y., Yuan, C.A., et al. (2002). Resistance of alpha-synuclein null mice to the parkinsonian neurotoxin MPTP. Proc. Natl. Acad. Sci. U S A *99*, 14524–14529.

David, S., Bucchieri, F., Corrao, S., Czarnecka, A.M., Campanella, C., Farina, F., Peri, G., Tomasello, G., Sciumè, C., Modica, G., et al. (2013). Hsp10: anatomic distribution, functions, and involvement in human disease. Front. Biosc. (Elite Ed.) *5*, 768–778.

de Oliveira, R.M., Vicente Miranda, H., Francelle, L., Pinho, R., Szegö, É.M., Martinho, R., Munari, F., Lázaro, D.F., Moniot, S., Guerreiro, P., et al. (2017). The mechanism of sirtuin 2–mediated exacerbation of alpha-synuclein toxicity in models of Parkinson disease. PLoS Biol. *15*, e2000374.

Di Maio, R., Barrett, P.J., Hoffman, E.K., Barrett, C.W., Zharikov, A., Borah, A., Hu, X., McCoy, J., Chu, C.T., Burton, E.A., et al. (2016). α-Synuclein binds to TOM20 and inhibits mitochondrial protein import in Parkinson's disease. Sci. Transl. Med. *8*, 342ra78.

Diógenes, M.J., Dias, R.B., Rombo, D.M., Vicente Miranda, H., Maiolino, F., Guerreiro, P., Näsström, T., Franquelim, H.G., Oliveira, L.M., Castanho, M.A., et al. (2012). Extracellular alpha-synuclein oligomers modulate synaptic transmission and impair LTP via NMDA-receptor activation. J. Neurosci. *32*, 11750–11762.

Du, Y., Wang, F., Zou, J., Le, W., Dong, Q., Wang, Z., Shen, F., Yu, L., and Li, Y. (2014). Histone deacetylase 6 regulates cytotoxic α-synuclein accumulation through induction of the heat shock response. Neurobiol. Aging *35*, 2316–2328.

Dunkley, P.R., Jarvie, P.E., and Robinson, P.J. (2008). A rapid Percoll gradient procedure for preparation of synaptosomes. Nat. Protoc. *3*, 1718–1728.

Fan, W., Fan, S.S., Feng, J., Xiao, D., Fan, S., and Luo, J. (2017). Elevated expression of HSP10 protein inhibits apoptosis and associates with poor prognosis of astrocytoma. PLoS ONE *12*, e0185563.

Faustini, G., Bono, F., Valerio, A., Pizzi, M., Spano, P., and Bellucci, A. (2017). Mitochondria and α-synuclein: friends or foes in the pathogenesis of Parkinson's disease? Genes (Basel) *8*, E377.

Fernandes, J.T.S., Tenreiro, S., Gameiro, A., Chu, V., Outeiro, T.F., and Conde, J.P. (2014). Modulation of alpha-synuclein toxicity in yeast using a novel microfluidic-based gradient generator. Lab Chip *14*, 3949–3957.

Fountaine, T.M., and Wade-Martins, R. (2007). RNA interference-mediated knockdown of α-synuclein protects human dopaminergic neuroblastoma cells from MPP(+) toxicity and reduces dopamine transport. J. Neurosci. Res. *85*, 351–363.

Ganguly, U., Chakrabarti, S.S., Kaur, U., Mukherjee, A., and Chakrabarti, S. (2018). Alpha-synuclein, proteotoxicity and Parkinson's disease: search for neuroprotective therapy. Curr. Neuropharmacol. *16*, 1086–1097.

Gao, X., Carroni, M., Nussbaum-Krammer, C., Mogk, A., Nillegoda, N.B., Szlachcic, A., Guilbride, D.L., Saibil, H.R., Mayer, M.P., and Bukau, B. (2015). Human Hsp70 disaggregase reverses Parkinson's-linked α-synuclein amyloid fibrils. Mol. Cell *59*, 781–793.

Groveman, B.R., Orrù, C.D., Hughson, A.G., Raymond, L.D., Zanusso, G., Ghetti, B., Campbell, K.J., Safar, J., Galasko, D., and Caughey, B. (2018). Rapid and ultra-sensitive quantitation of disease-associated α-synuclein seeds in brain and cerebrospinal fluid by αSyn RT-QuIC. Acta Neuropathol. Commun. *6*, 7.

Guardia-Laguarta, C., Area-Gomez, E., Rüb, C., Liu, Y., Magrané, J., Becker, D., Voos, W., Schon, E.A., and Przedborski, S. (2014). α-Synuclein is localized to mitochondria-associated ER membranes. J. Neurosci. *34*, 249–259.

Hansen, J.J., Bross, P., Westergaard, M., Nielsen, M.N., Eiberg, H., Børglum, A.D., Mogensen, J., Kristiansen, K., Bolund, L., and Gregersen, N. (2003). Genomic structure of the human mitochondrial chaperonin genes: HSP60 and HSP10 are localised head to head on chromosome 2 separated by a bidirectional promoter. Hum. Genet. *112*, 71–77.

Hashimoto, M., Hsu, L.J., Xia, Y., Takeda, A., Sisk, A., Sundsmo, M., and Masliah, E. (1999). Oxidative stress induces amyloid-like aggregate formation of NACP/alpha-synuclein in vitro. Neuroreport *10*, 717–721.

Hickey, R.W., Zhu, R.L., Alexander, H.L., Jin, K.L., Stetler, R.A., Chen, J., Kochanek, P.M., and Graham, S.H. (2000). 10 kD mitochondrial matrix heat shock protein mRNA is induced following global brain ischemia in the rat. Brain Res. Mol. Brain Res. *79*, 169–173.

Horvath, I., Iashchishyn, I.A., Moskalenko, R.A., Wang, C., Wärmländer, S.K.T.S., Wallin, C., Gräslund, A., Kovacs, G.G., and Morozova-Roche, L.A. (2018). Co-aggregation of pro-inflammatory S100A9 with α-synuclein in Parkinson's disease: ex vivo and in vitro studies. J. Neuroinflammation *15*, 172.

Horwich, A.L., Fenton, W.A., Chapman, E., and Farr, G.W. (2007). Two families of chaperonin: physiology and mechanism. Annu. Rev. Cell Dev. Biol. *23*, 115–145.

Hu, D., Sun, X., Liao, X., Zhang, X., Zarabi, S., Schimmer, A., Hong, Y., Ford, C., Luo, Y., and Qi, X. (2019). Alpha-synuclein suppresses mitochondrial protease ClpP to trigger mitochondrial oxidative damage and neurotoxicity. Acta Neuropathol. *137*, 939–960.

Kahle, P.J., Neumann, M., Ozmen, L., Muller, V., Jacobsen, H., Schindzielorz, A., Okochi, M., Leimer, U., van Der Putten, H., Probst, A., et al. (2000). Subcellular localization of wild-type and Parkinson's disease-associated mutant alpha-synuclein in human and transgenic mouse brain. J. Neurosc. *20*, 6365–6373.

Kim, S.-W., and Lee, J.-K. (2007). NO-induced downregulation of HSP10 and HSP60 expression in the postischemic brain. J. Neurosci. Res. *85*, 1252–1259.

Kramer, M.L., and Schulz-Schaeffer, W.J. (2007). Presynaptic alpha-synuclein aggregates, not Lewy bodies, cause neurodegeneration in dementia with Lewy bodies. J. Neurosci. *27*, 1405–1410.

Lázaro, D.F., Rodrigues, E.F., Langohr, R., Shahpasandzadeh, H., Ribeiro, T., Guerreiro, P., Gerhardt, E., Kröhnert, K., Klucken, J., Pereira, M.D., et al. (2014). Systematic comparison of the effects of alpha-synuclein mutations on its oligomerization and aggregation. PLoS Genet. *10*, e1004741.

Leverenz, J.B., Umar, I., Wang, Q., Montine, T.J., McMillan, P.J., Tsuang, D.W., Jin, J., Pan, C., Shin, J., Zhu, D., and Zhang, J. (2007). Proteomic identification of novel proteins in cortical Lewy bodies. Brain Pathol. *17*, 139–145.

Nakamura, K., Nemani, V.M., Wallender, E.K., Kaehlcke, K., Ott, M., and Edwards, R.H. (2008). Optical reporters for the conformation of alpha-synuclein reveal a specific interaction with mitochondria. J. Neurosci. *28*, 12305–12317.

Nakamura, K., Nemani, V.M., Azarbal, F., Skibinski, G., Levy, J.M., Egami, K., Munishkina, L., Zhang, J., Gardner, B., Wakabayashi, J., et al. (2011). Direct membrane association drives mitochondrial fission by the Parkinson disease-associated protein alpha-synuclein. J. Biol. Chem. *286*, 20710–20726.

Nakata, Y., Yasuda, T., Fukaya, M., Yamamori, S., Itakura, M., Nihira, T., Hayakawa, H., Kawanami, A., Kataoka, M., Nagai, M., et al. (2012). Accumulation of α-synuclein triggered by presynaptic dysfunction. J. Neurosci. *32*, 17186–17196.

Nesvizhskii, A.I., Keller, A., Kolker, E., and Aebersold, R. (2003). A statistical model for identifying proteins by tandem mass spectrometry. Anal. Chem. *75*, 4646–4658.

Nisemblat, S., Yaniv, O., Parnas, A., Frolow, F., and Azem, A. (2015). Crystal structure of the human mitochondrial chaperonin symmetrical football complex. Proc. Natl. Acad. Sci. U S A *112*, 6044–6049.

Oh, S.H., Lee, S.C., Kim, D.Y., Kim, H.N., Shin, J.Y., Ye, B.S., and Lee, P.H. (2017). Mesenchymal stem cells stabilize axonal transports for autophagic clearance of α-synuclein in Parkinsonian models. Stem Cells *35*, 1934–1947.

Orrú, C.D., Groveman, B.R., Hughson, A.G., Zanusso, G., Coulthart, M.B., and Caughey, B. (2015). Rapid and sensitive RT-QuIC detection of human Creutzfeldt-Jakob disease using cerebrospinal fluid. MBio *6*, e02451-14.

Ott, C., Martens, H., Hassouna, I., Oliveira, B., Erck, C., Zafeiriou, M.P., Peteri, U.K., Hesse, D., Gerhart, S., Altas, B., et al. (2015). Widespread expression of erythropoietin receptor in brain and its induction by injury. Mol. Med. *21*, 803–815.

Oueslati, A. (2016). Implication of alpha-synuclein phosphorylation at S129 in synucleinopathies: what have we learned in the last decade? J. Parkinsons Dis. *6*, 39–51.

Outeiro, T.F., Klucken, J., Strathearn, K.E., Liu, F., Nguyen, P., Rochet, J.C., Hyman, B.T., and McLean, P.J. (2006). Small heat shock proteins protect against alpha-synuclein-induced toxicity and aggregation. Biochem. Biophys. Res. Commun. *351*, 631–638.

Outeiro, T.F., Putcha, P., Tetzlaff, J.E., Spoelgen, R., Koker, M., Carvalho, F., Hyman, B.T., and McLean, P.J. (2008). Formation of toxic oligomeric α-synuclein species in living cells. PLoS ONE *3*, e1867.

Paiva, I., Jain, G., Lázaro, D.F., Jerčić, K.G., Hentrich, T., Kerimoglu, C., Pinho, R., Szegő, È.M., Burkhardt, S., Capece, V., et al. (2018). Alpha-synuclein deregulates the expression of COL4A2 and impairs ER-Golgi function. Neurobiol. Dis. *119*, 121–135.

Parker, W.D., Jr., Boyson, S.J., and Parks, J.K. (1989). Abnormalities of the electron transport chain in idiopathic Parkinson's disease. Ann. Neurol. *26*, 719–723.

Pathak, D., Berthet, A., Bendor, J.T., Yu, K., Sellnow, R.C., Orr, A.L., Nguyen, M.K., Edwards, R.H., Manfredsson, F.P., and Nakamura, K. (2017). Loss of α-synuclein does not affect mitochondrial bioenergetics in rodent neurons. eNeuro *4*, ENEURO.0216-16.2017.

Pinho, R., Paiva, I., Jercic, K.G., Fonseca-Ornelas, L., Gerhardt, E., Fahlbusch, C., Garcia-Esparcia, P., Kerimoglu, C., Pavlou, M.A.S., Villar-Piqué, A., et al. (2019). Nuclear localization and phosphorylation modulate pathological effects of Alpha-synuclein. Hum. Mol. Genet. *28*, 31–50.

Pozo Devoto, V.M., Dimopoulos, N., Alloatti, M., Pardi, M.B., Saez, T.M., Otero, M.G., Cromberg, L.E., Marín-Burgin, A., Scassa, M.E., Stokin, G.B., et al. (2017). αSynuclein control of mitochondrial homeostasis in human-derived neurons is disrupted by mutations associated with Parkinson's disease. Sci. Rep. *7*, 5042.

Rangaraju, V., Calloway, N., and Ryan, T.A. (2014). Activity-driven local ATP synthesis is required for synaptic function. Cell *156*, 825–835.

Rizzolo, K., Kumar, A., Kakihara, Y., Phanse, S., Minic, Z., Snider, J., Stagljar, I., Zilles, S., Babu, M., and Houry, W.A. (2018). Systems analysis of the genetic interaction network of yeast molecular chaperones. Mol. Omics *14*, 82–94.

Robson, E., Tweedy, C., Manzanza, N., Taylor, J.P., Atkinson, P., Randall, F., Reeve, A., Clowry, G.J., and LeBeau, F.E.N. (2018). Impaired fast network oscillations and mitochondrial dysfunction in a mouse model of alpha-synucleinopathy (A30P). Neuroscience *377*, 161–173.

Rockenstein, E., Mallory, M., Hashimoto, M., Song, D., Shults, C.W., Lang, I., and Masliah, E. (2002). Differential neuropathological alterations in transgenic mice expressing alpha-synuclein from the platelet-derived growth factor and Thy-1 promoters. J. Neurosci. Res. *68*, 568–578.

Schapira, A.H.V., Cooper, J.M., Dexter, D., Jenner, P., Clark, J.B., and Marsden, C.D. (1989). Mitochondrial complex I deficiency in Parkinson's disease. Lancet *333*, 1269.

Schmidt, C., Hesse, D., Raabe, M., Urlaub, H., and Jahn, O. (2013). An automated in-gel digestion/iTRAQ-labeling workflow for robust quantification of gel-separated proteins. Proteomics *13*, 1417–1422.

Scudamore, O., and Ciossek, T. (2018). Increased oxidative stress exacerbates α-synuclein aggregation in vivo. J. Neuropathol. Exp. Neurol. *77*, 443–453.

Silva, J.C., Gorenstein, M.V., Li, G.Z., Vissers, J.P., and Geromanos, S.J. (2006). Absolute quantification of proteins by LCMSE: a virtue of parallel MS acquisition. Mol. Cell. Proteomics *5*, 144–156.

Smith, G.M., and Gallo, G. (2018). The role of mitochondria in axon development and regeneration. Dev. Neurobiol. *78*, 221–237.

Song, W., Patel, A., Qureshi, H.Y., Han, D., Schipper, H.M., and Paudel, H.K. (2009). The Parkinson disease-associated A30P mutation stabilizes α-synuclein against proteasomal degradation triggered by heme oxygenase-1 overexpression in human neuroblastoma cells. J. Neurochem. *110*, 719–733.

Szegő, É.M., Gerhardt, E., Kermer, P., and Schulz, J.B. (2012). A30P α-synuclein impairs dopaminergic fiber regeneration and interacts with L-DOPA replacement in MPTP-treated mice. Neurobiol. Dis. *45*, 591–600.

Szegő, É.M., Gerhardt, E., and Outeiro, T.F. (2017). Sirtuin 2 enhances dopaminergic differentiation via the AKT/GSK-3β/β-catenin pathway. Neurobiol. Aging *56*, 7–16.

Tabner, B.J., Turnbull, S., King, J.E., Benson, F.E., El-Agnaf, O.M., and Allsop, D. (2006). A spectroscopic study of some of the peptidyl radicals formed following hydroxyl radical attack on beta-amyloid and alpha-synuclein. Free Radic. Res. *40*, 731–739.

Tang, W., Ehrlich, I., Wolff, S.B., Michalski, A.M., Wölfl, S., Hasan, M.T., Lüthi, A., and Sprengel, R. (2009). Faithful expression of multiple proteins via 2A-peptide self-processing: a versatile and reliable method for manipulating brain circuits. J. Neurosci. *29*, 8621–8629.

Tang, H., Chen, Y., Liu, X., Wang, S., Lv, Y., Wu, D., Wang, Q., Luo, M., and Deng, H. (2016). Downregulation of HSP60 disrupts mitochondrial proteostasis to promote tumorigenesis and progression in clear cell renal cell carcinoma. Oncotarget *7*, 38822–38834.

van Rumund, A., Green, A.J.E., Fairfoul, G., Esselink, R.A.J., Bloem, B.R., and Verbeek, M.M. (2019). α-Synuclein real-time quaking-induced conversion in the cerebrospinal fluid of uncertain cases of parkinsonism. Ann. Neurol. *85*, 777–781.

Vicente Miranda, H., Szego, É.M., Oliveira, L.M.A., Breda, C., Darendelioglu, E., de Oliveira, R.M., Ferreira, D.G., Gomes, M.A., Rott, R., Oliveira, M., et al. (2017). Glycation potentiates α-synuclein-associated neurodegeneration in synucleinopathies. Brain *140*, 1399–1419.

Villar-Piqué, A., Lopes da Fonseca, T., Sant'Anna, R., Szegö, É.M., Fonseca-Ornelas, L., Pinho, R., Carija, A., Gerhardt, E., Masaracchia, C., Abad Gonzalez, E., et al. (2016). Environmental and genetic factors support the dissociation between α-synuclein aggregation and toxicity. Proc. Natl. Acad. Sci. U S A *113*, E6506–E6515.

Volpicelli-Daley, L.A., Luk, K.C., and Lee, V.M.-Y. (2014). Addition of exogenous α-synuclein preformed fibrils to primary neuronal cultures to seed recruitment of endogenous α-synuclein to Lewy body and Lewy neurite-like aggregates. Nat. Protoc. *9*, 2135–2146.

Wang, X., Becker, K., Levine, N., Zhang, M., Lieberman, A.P., Moore, D.J., and Ma, J. (2019). Pathogenic alpha-synuclein aggregates preferentially bind to mitochondria and affect cellular respiration. Acta Neuropathol. Commun. *7*, 41.

Xia, Q., Liao, L., Cheng, D., Duong, D.M., Gearing, M., Lah, J.J., Levey, A.I., and Peng, J. (2008). Proteomic identification of novel proteins associated with Lewy bodies. Front. Biosci. *13*, 3850–3856.

Xiong, R., Zhou, W., Siegel, D., Kitson, R.R., Freed, C.R., Moody, C.J., and Ross, D. (2015). A novel Hsp90 inhibitor activates compensatory heat shock protein responses and autophagy and alleviates mutant A53T α-synuclein toxicity. Mol. Pharmacol. *88*, 1045–1054.

Yin, G., Lopes da Fonseca, T., Eisbach, S.E., Anduaga, A.M., Breda, C., Orcellet, M.L., Szegő, É.M., Guerreiro, P., Lázaro, D.F., Braus, G.H., et al. (2014). α-Synuclein interacts with the switch region of Rab8a in a Ser129 phosphorylation-dependent manner. Neurobiol. Dis. *70*, 149–161.

Ysselstein, D., Dehay, B., Costantino, I.M., McCabe, G.P., Frosch, M.P., George, J.M., Bezard, E., and Rochet, J.C. (2017). Endosulfine-alpha inhibits membrane-induced α-synuclein aggregation and protects against α-synuclein neurotoxicity. Acta Neuropathol. Commun. *5*, 3.

Zambon, F., Cherubini, M., Fernandes, H.J.R., Lang, C., Ryan, B.J., Volpato, V., Bengoa-Vergniory, N., Vingill, S., Attar, M., Booth, H.D.E., et al. (2019). Cellular α-synuclein pathology is associated with bioenergetic dysfunction in Parkinson's iPSC-derived dopamine neurons. Hum. Mol. Genet. *28*, 2001–2013.

STAR★METHODS

KEY RESOURCES TABLE

REAGENT or RESOURCE	SOURCE	IDENTIFIER
Antibodies		
Mouse monoclonal anti-β-Actin (Clone AC-15)	Sigma-Aldrich	Cat#A5441; RRID: AB_476744
Mouse monoclonal anti-BiP	BD Biosciences	Cat#610978; RRID: AB_398291
Mouse monoclonal anti-DRP1/2	Abcam	Cat#ab56788; RRID: AB_941306
Mouse monoclonal anti-Flag M2	Sigma-Aldrich	Cat#F1804; RRID: AB_262044
Rabbit polyclonal anti-Flag	Sigma-Aldrich	Cat#F7425; RRID: AB_439687
Mouse monoclonal anti-GADD 153 (Clone B-3)	Santa Cruz Biotechnology	Cat#sc-7351; RRID: AB_627411
Rabbit monoclonal anti-GAPDH (Clone 14C10)	Cell Signaling Technology	Cat#2118S; RRID: AB_561053
Mouse monoclonal anti-GFP (Clones 7.1 and 13.1)	Roche	Cat#11814460001; RRID: AB_390913
Rabbit polyclonal anti-GFP (Clone FL)	Santa Cruz Biotechnology	Cat#sc-8334; RRID: AB_641123
Rabbit polyclonal anti-HSP 10 (Clone FL-102)	Santa Cruz Biotechnology	Cat#sc-20958, RRID: AB_2279780
Mouse monoclonal anti-HSP10 (Clone D-8)	Santa Cruz Biotechnology	Cat#sc-376313; RRID: AB_10988238
Rabbit polyclonal anti-HSP 60 (Clone H-300)	Santa Cruz Biotechnology	Cat#sc-13966; RRID: AB_2121457
Rabbit polyclonal anti-HTRA2	R and D Systems	Cat#AF1458; RRID: AB_2280094
Rabbit polyclonal anti-MAP2	Abcam	Cat#ab32454; RRID: AB_776174
Rabbit monoclonal anti-PSD95 (Clone D27E11)	Cell Signaling Technology	Cat#3450S; RRID: AB_2292883
Goat polyclonal anti-SOD-1 (Clone C-17)	Santa Cruz Biotechnology	Cat#sc-8637; RRID: AB_2193781
Rabbit polyclonal anti-SOD	Millipore	Cat#06-984; RRID: AB_310325
Rabbit polyclonal anti-Synapsin 1/2	Synaptic Systems	Cat# 106 002; RRID:AB_887804
Mouse monoclonal anti-Synaptophysin	Sigma-Aldrich	Cat#S5768; RRID: AB_477523
Mouse monoclonal anti-a-Synuclein	BD Biosciences	Cat#610787; RRID: AB_398108
Rabbit polyclonal anti-alpha-Synuclein (C-20)-R	Santa Cruz Biotechnology	Cat#sc-7011-R; RRID: AB_2192953
Rabbit monoclonal anti-alpha-Synuclein (Clone MJFR1)	Abcam	Cat#ab138501; RRID: AB_2537217
Mouse monoclonal anti-aggregated-a-Synuclein (Clone 5G4)	Millipore	Cat#MABN389; RRID: AB_2716647
Rat monoclonal anti-a-Synuclein (human) (Clone 15G7)	Enzo Life Sciences	Cat#ALX-804-258-LC05; RRID: AB_11180660
Mouse monoclonal anti-phosphorylated α-Synuclein (pSyn#64)	Wako	Cat#015-25191; RRID: AB_2537218
Mouse monoclonal anti-Tyrosine hydroxylase	Sigma-Aldrich	Cat#T2928; RRID: AB_477569
Rabbit polyclonal anti-Tyrosine Hydroxylase	Millipore	Cat#AB152; RRID: AB_390204
Bacterial and Virus Strains		
EF1-aSYN-T2A-GFP (125,126)	This paper	N/A
FUGW-(h)HSPE1-Flag (292)	This paper	N/A
FUGW-Mito-dsRed2 (284)	This paper	N/A
Biological Samples		
Human brain samples from patients with DLB	University of Newcastle Brain Tissue Resource	https://nbtr.ncl.ac.uk/
Chemicals, Peptides, and Recombinant Proteins		
Penicilin-Streptomycin	PAN Biotech	Cat#P06-07100
Cytosine 1-β-D-arabinofuranoside	Sigma-Aldrich	Cat#C1768-1G
Oligomycin	Sigma-Aldrich	Cat#O4876-25MG
FCCP	Sigma-Aldrich	Cat#2920
Rotenone	Sigma-Aldrich	Cat#R8875

(*Continued on next page*)

Continued

REAGENT or RESOURCE	SOURCE	IDENTIFIER
Antimycin A	Sigma-Aldrich	Cat#A8674-25MG
Tetraethylbenzimidazolylcarbocyanine iodide (JC-1)	Thermo Fisher Scientific	*Cat#M34152*
Calcein AM	Thermo Fisher Scientific	Cat#C3100MP
Ionomycin	Sigma-Aldrich	Cat#I9657
Dichlorodihydrofluorescein diacetate (DCFH-DA)	Sigma-Aldrich	Cat#D6883
MitoSOX	Thermo Fisher Scientific	Cat#M36008
1-thio-β-D-galactopyranoside	Peqlab	N/A
Critical Commercial Assays		
HSP60/HSP10 Glow-Fold Protein Refolding Kit	R&D Systems	Cat#K-300
Duolink *In Situ* Detection Reagents Orange	Sigma-Aldrich	Cat#DUO92007
Deposited Data		
UniProtKB/Swiss-Prot mouse proteome (UniProtKB release 2017_11, 16944 entries)	This paper	ftp://pir17.georgetown.edu/pub/databases/uniprot/previous_releases/release-2017_11/knowledgebase/UniProtKB_SwissProt-relstat.html
Experimental Models: Cell Lines		
pT7-7 h aSyn in BL21 cells	This paper	N/A
pET21A HspE1 in BL21 cells	This paper	N/A
Experimental Models: Organisms/Strains		
Wistar E18 rat embryos	This paper	N/A
WTaSyn mouse	This paper	Rockenstein et al., 2002; PMID 12111846
A30PaSyn mouse	This paper	Kahle et al., 2000; PMID 10964942
C57BL/6J mouse	Charles River	C57BL/6J
Oligonucleotides		
BglII-KOZAK-WT Forward: 5′-GGCAGATCTACCGG TCGCCACCATGGATGTATTCATGAAAGGACTTTCA AAGGCCAAGGAGGG-3′	This paper	N/A
Not-syn wo STOP reverse: 5′-CCCGCGGCCGCGG CTTCAGGTTCGTAGTCTTGATAC-3′	This paper	N/A
BamH1-Kozak-(H) HSPE1 Forward: 5′-GGGGGAT CCGCCGCCACCATGGCAGGACAAGCGTTTAG AAAG-3′	This paper	N/A
EcoR1-Flag Reverse: 5′-CCCGAATTCTTACTTA TCGTCGTCATCCTTGTAATC-3′	This paper	N/A
Data, software and Algorithms		
Raw MS data	This paper	https://doi.org/10.5281/zenodo.3255277
ProteOn analysis software	Bio-Rad	Cat# 176-0200
XFe96 analyzer	Agilent Technologies	Wave Controller 2.4
Excalibur 2.4 software	Excalibur Systems	https://www.mil-1553.com/software
Raw2MSMS software v1.17	Max Planck Institute for Biochemistry, Martinsried, Germany	N/A
MASCOT 2.4 software	Matrixscience	http://www.matrixscience.com/mascot_support_v2_4.html
Scaffold software version 4.4.1.1	Proteome Software Inc.	http://www.proteomesoftware.com/products/scaffold/
Protein Prophet algorithm	Nesvizhskii Lab	Nesvizhskii et al., 2003, PMID:14632076
Excellence Imaging Software	Olympus Germany	
ImageJ JACoP plugin	NIH ImageJ	http://imagejdocu.tudor.lu/doku.php?id=plugin:analysis:jacop_2.0:just_another_colocalization_plugin:start

(*Continued on next page*)

Continued

REAGENT or RESOURCE	SOURCE	IDENTIFIER
Power analysis (G Power)	Duesseldorf University	http://www.gpower.hhu.de/
R software packages version 2.8.0	R Development Core Team 2008	https://www.r-project.org/
ProteinLynx Global Server version 3.0.2	Waters Cooperation	http://www.waters.com/waters/de_DE/ProteinLynx-Global-SERVER-%28PLGS%29/nav.htm?cid=513821&locale=de_DE

LEAD CONTACT AND MATERIALS AVAILABILITY

Further information and requests for reagents may be directed to and will be fulfilled by the corresponding author Tiago F. Outeiro (touteir@gwdg.de).

EXPERIMENTAL MODEL AND SUBJECT DETAILS

Ethical statement and animal lines

Animal procedures were performed in accordance with the European Community (Directive 2010/63/EU), institutional and national guidelines (Landesamt für Verbraucherschutz, Braunschweig, Lower Saxony, Germany, license number: 33.9-42502-04-17/2413). All mice were housed at controlled temperature and 12:12 h light/dark cycle. Number of animals included in the analysis was estimated by power analysis (R software packages, Vienna, Austria), and selection of animals was randomized. Mice that lost more than 20% of the body weight during the treatment were excluded from the experiment. Young (2-3 months old) and middle-age (5-7 months old) wild-type (DBA/2F1 (DBA; control of WTaSyn) or C567BL/6J (Bl6; control of A30PaSyn) and human aSyn-expressing mice (Thy-1 promoter; WT or A30P human aSyn (Kahle et al., 2000; Rockenstein et al., 2002; Szegő et al., 2012)) were used in the study. Only male mice, or female and male mice mixed groups (only for lentivirus injection) were used.

Patients and controls

Human brain samples from patients with PD or DLB, and control individuals were obtained from the Newcastle Brain Tissue Resource (NBTR) or from the Regional Ethical Review Board of Lund University, Sweden (2014/631). Samples were classified according to the disease diagnostics and were anonymized, information about age, sex and post-mortal delay are indicated in Table S2. The use of human material was approved by the Ethics Committee for Using Human Brain Samples for Fundamental Research, University Medical Center, Göttingen.

METHOD DETAILS

Lentivirus injections and tissue dissection

To inject lentivirus, only young (2-4 months old) female and male mice were used. Two times 0.5 μl lentivirus (adjusted to $1x10^7$ TU/ml) were injected in the substantia nigra of both hemispheres (de Oliveira et al., 2017). One month after the injection, brain tissue was rapidly dissected for mitochondrial assays and protein analysis and processed immediately. For immunofluorescence analysis, brains were fixed in 4% PFA, and after cryoprotection (30% sucrose), 30 μm coronal sections were cut.

Primary neuronal culture

Primary neuronal cultures (prepared from E18 Wistar rat embryos, mixed sex) were infected with lentivirus coding GFP, WTaSyn or A30PaSyn on day 4 (MOI 1), and with GFP or HSP10-Flag on day 7 (MOI 1). Cells were maintained in Neurobasal supplemented with B27 and 2mM glutamax (Villar-Piqué et al., 2016; Szegő et al., 2017).

Constructs

Full-length human aSyn cDNA (SNCA, gene association NM000345- WT and A30P mutation) was sub cloned into a 3rd-generation lentiviral vector CD526A-1, followed by a T2A-GFP sequence, under the original vector promoter (EF1α). The inserts (aSyn, WT and A30P mutation) including the Kozak sequence have been generated by PCR. The CD526A-1 vector containing only the T2A-GFP cassette was used for control experiments. The T2A sequence is cleaved after translation, generating two proteins from a single open reading frame and resulting in stoichiometric expression of the gene of interest and the fluorescent reporter (Tang et al., 2009).

Full-length human heat shock protein family E (HSP10) member 1 (HSPE1, gene association NM 0022157.2) was sub cloned into a 3rd-generation lentiviral plasmid with hUbC-driven EGFP, where the original GFP cassette has been replaced by the HSPE1 gene including the Kozak sequence and a C-terminal Flag tag. The FUGW vector containing only the GFP cassette was used for control experiments.

Cell lysis, tissue fractionation, western blotting and immunoprecipitation

For protein quantification and detection of Triton X-100 insoluble proteins, cells were lysed in 1% Triton X-100. After centrifugation (14 000 g, 30 min), supernatant was used as Triton X-100 soluble, the pellet as Triton X-100 insoluble fraction. For immunoblotting, tissue samples or cells were collected and homogenized in RIPA buffer (50 mM Tris, pH 8.0, 0.15 M NaCl, 0.1% SDS, 1.0% NP-40, 0.5% Na-Deoxycholate, 2 mM EDTA, supplemented with Complete Protease Inhibitor Cocktail (Roche, Mannheim, Germany)), for co-immunoprecipitation (co-IP) assay, in IP buffer (50 mM Tris-HCl pH 7.5; 0.5 mM EDTA; 150 mM NaCl; 0.05% NP40) supplemented with inhibitor cocktail. In each IP sample, 150 μg of total protein lysate was pre-cleared (20 μl of protein G beads (Invitrogen, Barcelona, Spain) for 30 min at 4°C; the beads were later treated as the lysates and used as IgG controls) and then incubated with 2 μg of one the IP antibodies (aSyn (BD) or HSP-10 (Santa Cruz)) overnight at 4°C. Then samples were mixed with 15 μl protein G beads and incubated for 3 h. Beads were washed 6 times with IP buffer, and proteins were eluted by using 3x 150 μl acidic buffer (0.2 M glycine pH 2.4). Eluates were then precipitated with trichloric acid, resuspended in 50 μl protein sample buffer (125 mM Tris-HCl, 4% SDS 0,5% Bromophenol blue, 4 mM EDTA, 20% Glycerol, 10% β-mercapto-ethanol, pH 6.8) and boiled. Proteins from 10 μg lysate as input or from 10 μl of the supernatants of IP were separated via SDS-PAGE gel and then transferred onto nitrocellulose membrane. After blocking, membranes were first incubated in the presence of one of the primary antibodies (aSyn, HSP10, Flag, GADD153, HtrA2, HSP60, paSyn, hmaSyn, SOD2, synaptophysin, PSD95, TH, actin, GAPDH) and then with IRDye 800CW or 680LT (Li-Cor, Bad Homburg, Germany), respectively. Membranes were imaged using Li-Cor Odyssey CLx imaging system. Intensities of specific bands were normalized. Synaptosomes, total mitochondria and cytosolic fractions were prepared from the same brain as described below (Dunkley et al., 2008), from young and middle-age mice. Briefly, striatal samples were homogenized in isotonic sucrose solution (320 mM sucrose, 1 mM EDTA, 5 mM TRIS, 250 μM DTT, pH 7,4), nuclei and non-lysed tissue was pelleted (1000 g, 5 min), then supernatant was separated on Percoll gradient. (31 000 g, 4°C, 20 min). Synaptosomal fraction was collected from the band between buffer containing 23% and 15% Percoll, respectively. Mitochondria fractions were collected after centrifugation of the nuclei-pelleted lysate at 6000 g. Collected fractions were washed in assay buffer (synaptosome: 3.5mM KCl, 120mM NaCl, 1.3mM $CaCl_2$, 0.4 mM KH_2PO_4, 1.2 mM Na_2SO_4, 15 mM D-glucose, 10 mM pyruvate, 0.4% (w/v) fatty acid-free bovine serum albumin, 10 mM TES (N- [tris(hydroxymethyl)methyl]-2-aminoethanesulfonic acid), pH 7.4.; mitochondria: 70 mM sucrose, 210 mM mannitol, 5.0 mM HEPES, 1.0 mM EGTA, 0.5% (w/v) fatty acid free BSA, pH 7.2). 10 μg (Seahorse) or 50 μg (other mitochondrial assays) protein was used for biochemical assays (protein concentrations were determined by the Bradford assay (Bio-Rad)).

Mitochondrial assays

XF96 analyzer was used to measure respiration according to the manufacturer's instructions. Briefly, assay plates were coated before use with 0.0033% (v/v) polyethyleneimine solution (100μl/well) overnight at room temperature. Synaptosomes or mitochondria were attached by centrifugation (4000 g, 20 min, 4°C) to coated Seahorse plates (10 μg protein/well) or 96-well microplates (50 μg/well). This was followed by dye loading for biochemical assays, or direct measurement in the XF96 analyzer. Spare respiratory capacity (SRC) was calculated as the difference between the maximal (FCCP) and basal respiration. % change in SRC is the relative change compared to control SRC. Tetraethylbenzimidazolylcarbocyanine iodide (JC-1, 50 nM, 30 min loading at 37°C)) was used to measure mitochondrial membrane potential, according to manufacturer's instructions. Fluorescence (485/505 and 535/570) was detected with a plate reader (Infinite 200 Pro, Tecan). After measuring the basal potential, the mitochondrial uncoupler FCCP (1 μM) was used to detect stress-induced loss of mitochondrial membrane potential, and preparations were measured until the recovery in the control samples was complete. Mitochondrial permeability transition pore (mPTP) opening was measured by using Calcein AM (1 μM, in the presence of 1 μM $CoCl^2$; 30 min, 37°C), according to the instructions. Ionomycin (500 nM) treatment was used as positive control. Fluorescence was measured (494/517 nm) with a Tecan plate reader. Cytoplasmic and mitochondrial reactive oxygen species (ROS) were measured by using dichlorodihydrofluorescein diacetate (DCFH-DA; 10 μM, 37°C, 30 min) or MitoSOX (200 nM, 20 min, 37°C), according to the instructions. Fluorescence was measured with a plate reader (485/530 nm or 510/580 nm, respectively). To address stress-induced ROS production and removal, preparations were treated with 1% H_2O_2.

Recombinant aSyn and HSP10 expression and purification

pT7-7 h aSyn and pET21A HspE1 were transformed into competent BL21 (Sigma) cells. Bacteria were incubated in 2x LB medium at 37°C with shaking to an OD_{600} of 0.6. Recombinant protein expression was induced with 1 mM 1-thio-β-D-galactopyranoside (Peqlab) for 3 hours. Cells were harvested by centrifuging (6000 g, 20 min) and lysed (750 mM NaCl, 10 mM Tris, 1 mM EDTA pH 7.6, protease inhibitor (Roche, Mannheim, Germany)). The supernatant obtained after centrifugation (15 000 g, 20 min) was dialysed (10 mM Tris pH 7.6, 1 mM EDTA, 50 mM NaCl). For purification of recombinant HSP10, the supernatant was loaded onto an anion exchange column (HiTrap Q HP, GE Healthcare) equilibrated in 25 mM Tris, pH 7.6. The unbound fraction contained pure HSP10 that was concentrated using a centrifugation filter (3K, Amicon, Merck, Darmstadt, Germany) and stored at −80°C. For aSyn, the supernatant was purified with anion exchange chromatography (HiTrap Q HP, GE Healthcare, Solingen, Germany) using a constant gradient 0-1 mM NaCl followed by gel filtration (HiLoad Superdex 75, GE Healthcare). Pre-formed fibrils(Volpicelli-Daley et al., 2014) and oligomers(Diógenes et al., 2012) were prepared according to the published protocols.

HSP10/HSP60 protein refolding assay

HSP60/HSP10 Glow-Fold Protein Refolding Kit was used according to the manufacturer's instructions. Briefly, recombinant aSyn monomers, oligomers or pre-formed fibrils (PFFs) were mixed (final concentration in the reaction mixture 1 μM or 100 nM, respectively) with HSP10, HSP60 and Gold-Fold substrate protein in the presence of Mg^{2+}-ATP. The reaction mixture was incubated for 30 min, then, after 7 min heat shock (45°C), luminescence was measured in the presence of Luciferin Reagent (time 0, completely unfolded Gold-Fold substrate). The reaction mixture was further incubated at 30°C, and protein folding was tested every 30 min. In case of aSyn pretreatment, recombinant aSyn species were incubated first just with HSP10 for 30 min, then the rest of the mixture was added, as above. Reaction mixture of the negative control did not contain Mg^{2+}-ATP, reaction mixture of the "folding control" contained 0.15 μg/ml BSA instead of aSyn, the mixture of the positive control was not subjected to heat shock.

Surface-Plasmon Resonance (SPR) measurements

Interaction studies were performed by using the ProteOn XPR36 Protein Interaction Array system. Recombinant HSP10 was immobilized according to manufacturer's protocols on a GLH sensor chip by amino-coupling with a final immobilization level of ~12500 RU. Analytes were diluted in PBS Tween (0.005%) as running buffer. Samples were injected with a flow rate of 50 μl/min for 2 min. For referencing a ligand surface without any bound protein was used. Data correction was done by subtracting the blank chip surface from the protein bound surface to remove contribution of unspecific compounds on the chip surface. For obtaining the corresponding association and dissociation rate constants the 1:1 interaction model (ProteOn analysis software) was used for fitting the sensograms.

aSyn real time quaking-induced conversion (RT-QuiC)

RT-QuiC reactions were performed as described earlier(Orrú et al., 2015; Groveman et al., 2018). Briefly, 100 μl of reaction mixtures were pipetted in triplicates in black 96-well plates (Corning Incorporated, Washington, USA). The final composition of the reaction mixtures: 150 mM NaCl, 1 mM EDTA, 10 μM ThioT, 70 μM SDS, 10 μg/ml monomeric aSyn, 1 μg/ml fibrillar aSyn in PBS buffer (pH = 7.1), 1 μg/ml HSP10. Plates were covered with sealing tape and incubated in a plate reader (41°C, Infinite M200 fluorescence plate reader, Tecan, Hamburg, Germany) for 250 amplification cycles (1 min orbital shaking at 432 rpm; 2 min incubation; measurement of fluorescence intensity at 480 nm). Endpoint fluorescent intensities were normalized by baseline values.

Proteomic screen of Syn-interacting proteins

To identify aSyn-interacting proteins, mass spectrometric analyses were performed by the Core Facility Proteomics at the University Medical Center Göttingen (Nesvizhskii et al., 2003; Atanassov and Urlaub, 2013). Synaptosome lysates from the striatum (4-5 months old BDF, Bl6, WTaSyn and A30PaSyn mice) were pre-cleared and incubated in the presence of aSyn antibody (Yin et al., 2014; Szegő et al., 2017). Immunoprecipitated proteins were eluted in 1 × NuPAGE LDS Sample Buffer and separated on 4%–12% NuPAGE Novex Bis-Tris Minigels. Each lane was sliced into 23 parts, then reduced with dithiothreitol, alkylated with 2-iodoacetamide and digested with trypsin. The resulting peptide mixtures were dried, reconstituted in 2% acetonitrile/0.1% formic acid (Atanassov and Urlaub, 2013). Samples were enriched on a self-packed reversed phase-C18 precolumn (0.15 mm ID x 20 mm, Reprosil-Pur120 C18-AQ 5 μm) and separated on an analytical reversed phase-C18 column (0.075 mm ID x 200 mm, Reprosil-Pur 120 C18-AQ, 3 μm) using a 15 min linear gradient of 5%–35% acetonitrile/0.1% formic acid at 300 nl/min). The eluent was analyzed on a Q Exactive hybrid quadrupole/orbitrap mass spectrometer (Thermo Fisher Scientific) equipped with a FlexIon nanoSpray source and operated under Excalibur 2.4 software using a data-dependent acquisition method. Each experimental cycle was of the following form: one full MS scan across the 350-1600 m/z range was acquired at a resolution setting of 70 000 FWHM, and AGC target of $1x10^6$ and a maximum fill time of 60 ms. Up to the 10 most abundant peptide precursors of charge states 2 to 5 above a $2x10^4$ intensity threshold were then sequentially isolated at 2.0 FWHM isolation width, fragmented with nitrogen at a normalized collision energy setting of 25%, and the resulting product ion spectra recorded at a resolution setting of 17 500 FWHM, and AGC target of $2*10^5$ and a maximum fill time of 60 ms. Selected precursor m/z values were then excluded for the following 6 s. Peaklists were extracted from the raw data using Raw2MSMS software v1.17 (Max Planck Institute for Biochemistry, Martinsried, Germany). Protein identification was achieved using MASCOT 2.4 software (Matrixscience, London, United Kingdom). Proteins were identified against the UniProtKB mouse reference proteome v2014.02. The search was performed with trypsin as enzyme and iodoacetamide as cysteine blocking agent. Up to two missed tryptic cleavages and methionine oxidation as a variable modification were allowed for. Search tolerances were set to 10 ppm for the precursor mass and 0.05 Da for fragment masses, and ESI-QUAD-TOF specified as the instrument type. Scaffold software version 4.4.1.1 (Proteome Software Inc., Portland, OR) was used to validate MS/MS based peptide and protein identifications. Peptide identifications were accepted if they could be established at greater than 95% probability by the Percolator algorithm. Protein probabilities were assigned by the Protein Prophet algorithm (Nesvizhskii et al., 2003). Protein identifications were accepted if they could be established at greater than 99% by the Percolator algorithm and contained at least 2 identified peptides. Protein hits that contained similar peptides and could not be differentiated based on MS/MS analysis alone were grouped to satisfy the principles of parsimony. Proteins sharing significant peptide evidence were grouped into clusters.

Identification of HSP10 from cytoplasmic fractions by mass spectrometry

Gel electrophoreses were performed in parallel on precast NuPAGE 4%–12% Bis-Tris gradient gels using a MES buffer system according to the manufacturer (Thermo Fisher Scientific). Proteins were either visualized by colloidal Coomassie staining (gel 1) or transferred on nitrocellulose membranes and immunodetected as described below (gel 2). Gel regions of interest were identified by overlaying the images from colloidal Coomassie staining and immunodetection in the Delta 2D image analysis software (Decodon). Gel bands were excised manually and subjected to automated in-gel digestion with trypsin as described (Schmidt et al., 2013). Tryptic peptides were dried down in a vacuum centrifuge, re-dissolved 0.1% trifluoro acetic acid and spiked with 2.5 fmol/μL of yeast enolase 1 tryptic digest standard (Waters Corporation) for protein quantification according to the TOP3 method (Silva et al., 2006). Nanoscale reversed-phase UPLC separation and ion mobility-enhanced mass spectrometric analysis of tryptic peptides was performed with a Synapt G2-S QTOF LC-MS system (Waters Corporation) as described (Ott et al., 2015). A custom database was compiled by adding the sequence information for yeast enolase 1 and porcine trypsin to the UniProtKB/Swiss-Prot mouse proteome (UniProtKB release 2017_11, 16944 entries) and by appending the reversed sequence of each entry to enable the determination of false discovery rate (FDR). Precursor and fragment ion mass tolerances were automatically determined by ProteinLynx Global Server (version 3.0.2, Waters Cooperation) and were typically below 5 ppm for precursor ions and below 10 ppm (root mean square) for fragment ions. Carbamidomethylation of cysteine was specified as fixed and oxidation of methionine as variable modification. One missed trypsin cleavage was allowed. The FDR for protein identification was set to 1% threshold.

In situ Proximity Ligation Assay (PLA)

In situ PLA was performed according to manufacturer's protocol (DuoLink PLA, Sigma-Aldrich). Briefly, PFA-fixed primary neurons were permeabilized (0.5% Triton X-100, 10 min), blocked (2% BSA, 30 min, 37°C) and incubated with the primary antibodies (anti-HSP10 and anti-synuclein or anti-GFP and anti-synuclein). The experiment was performed with a pair of antibodies from different species. After washing with buffer (provided in the kit), cells were incubated with the PLA probes (secondary antibodies against two different species bound to two oligonucleotides: anti-mouse MINUS and anti-rabbit PLUS; 37°C, 60 min). Ligation of the oligonucleotide was performed after washing (37°C, 30 min) followed by an amplification step (37°C, 100 min) to label with fluorescent oligonucleotide and increase signal intensity. For every antibody, a negative control experiment was performed where only one antibody was incubated with the PLA probes.

Immunostainings, microscopy, and stereology

Fixed cells or brain slices were treated according to (Szegő et al., 2017), and then cells were incubated in the presence of one of the primary antibodies (see Key Resources Table, 24 h). Alexa Fluor 488, 555 or 633 (Invitrogen, Carlsbad, CA, USA) conjugated anti-mouse, anti-rabbit or anti-rat antibodies were used. Evaluation of the number of dopaminergic neurons in the substantia nigra after viral vector injection, was done as previously described (Szegő et al., 2017). Counts were performed manually and blinded for experimental grouping. After antigen retrieval (10 s formic acid, 10 min boiling in 10 mM citrate buffer; pH6) and quenching (H_2O_2), 6μm paraffin sections from human brain were incubated in the presence of primary antibody (see Key Resources Table, 24 h). Alexa Fluor 488 conjugated anti-mouse (1:200) and Alexa Fluor 594 conjugated anti rabbit (1:200) antibodies were used for 1 h. Fluorescent images were taken using an Olympus IX81-ZDC microscope with Excellence software. Exposure time was equal for the same staining across the experimental groups. Manders' coefficient was calculated by using ImageJ JACoP plugin. For confocal imaging, human brains were fixed (6% PFA, 1 month) and cryoprotected (20% sucrose). Regions were cut into coronal whole brain sections and small specimens. Basal ganglia and mesencephalon were separated cut into 40 μm thick sections. After washing and blocking (1% BSA, 5% normal donkey serum and 0.3% Triton X-100), free-floating sections were incubated first with primary antibodies (HSP10, Santa Cruz and aSyn, Santa Cruz; overnight, 4°C), then with fluorescence conjugated secondary antibodies (anti-mouse Alexa Fluor 488 and anti-rabbit Cy3 (Invitrogen), 2 h, room temperature). Fluorescent images were taken using an Olympus DP73 camera, driven by CellSens software. Confocal images were taken using Leica SP8 camera driven by Leica Application Suite X software.

QUANTIFICATION AND STATISTICAL ANALYSIS

Selection of animals or distribution of conditions in each experiment was randomized. Data collection was done blinded. Data was assessed for normality using the Shapiro–Wilk test, for equal variance using F test. Data were analyzed either with 1- or 2-way analysis of variance followed by Tukey's honestly significant difference test (Statistica, StatSoft, Tulsa, USA). % change in the SRC was analyzed after normalization, the individual animal and experimental numbers were used as random factor (Szegő et al., 2012). The null hypothesis was rejected at the 0.05 p value level. Data are presented as mean ± SD.

DATA AND CODE AVAILABILITY

Further information about the data may be directed to and will be fulfilled by the corresponding authors Éva M. Szegő (eva.szego@gmail.com) or Tiago F. Outeiro (touteir@gwdg.de). Raw data (mass spectrometry) can be found at https://doi.org/10.17632/x2gcnh7jjj.1.